
Run Procrustes, Run! On the convergence of accelerated Procrustes Flow

Anastasios Kyrillidis
IBM & Rice University
anastasios@rice.edu

Shashanka Ubaru
University of Minnesota-Twin Cities
ubaru001@umn.edu

Georgios Kollias
IBM
gkollias@us.ibm.com

Kristofer Bouchard
Lawrence Berkeley National lab
KEBouchard@lbl.gov

Abstract

In this work, we present theoretical results on the convergence of *non-convex* accelerated gradient descent in matrix factorization models. The technique is applied to matrix sensing problems with squared loss, for the estimation of a rank r optimal solution $X^* \in \mathbb{R}^{n \times n}$. We show that the acceleration leads to linear convergence rate, even under non-convex settings where the variable X is represented as UU^T for $U \in \mathbb{R}^{n \times r}$. Our result has the same dependence on the condition number of the objective –and the optimal solution– as that of the recent results on non-accelerated algorithms. However, acceleration is observed in practice, both in synthetic examples and in two real applications: neuronal multi-unit activities recovery from single electrode recordings, and quantum state tomography on quantum computing simulators.

1 Introduction

Accelerated versions of gradient descent (GD), inspired by Polyak [1] and Nesterov [2], are the methods of choice in various optimization tasks, including training deep neural networks (DNN) [3, 4, 5, 6, 7, 8]. Acceleration is based on *momentum*: as long as the iterates point to (approx.) the same direction, momentum from previous estimates “pushes” the sequence of estimates more aggressively along that path. This way, momentum allows faster decay on the objective landscape, empirically [2].

Despite its widespread use [9, 10, 11, 9, 12], theoretical results on why momentum works well are mostly restricted to the convex case, where it provably begets significant gains w.r.t. convergence rate [13, 14, 15, 16, 17, 18, 19]. Exceptions, beyond convexity, include (i) settings that involve non-convex (and structured) constraint sets [20, 21, 22], but with a convex objective; and (ii) works that consider generic non-convex settings but do not focus on globally solving the problem: they study whether acceleration leads to fast convergence to a critical point –saddle point or local minimum– of the problem criterion [23, 24, 25, 26, 27, 28].

In this work, we show that the success of momentum can be theoretically fleshed out in the context of shallow, linear neural networks. We consider low-rank factorization for the matrix sensing problem as our centric test case. Our work can be seen as a first step towards understanding momentum in general non-linear models, whose training objectives are more involved and complex. Such simplifications have been followed in other recent works in machine learning and theoretical computer science, such as the cases of convolutional neural networks [29], the effect of over-parameterization in training [30], and landscape characterization of generic objectives [31, 32, 33].

Our contributions can be summarized as follows:

- For *noiseless* matrix sensing, we prove that a heavy-ball-like method on the low-rank factors converges linearly to the optimal solution. Our framework borrows ideas from the two-step momentum approach in convex settings, as in [1, 2], and applies to the factorized gradient descent algorithm, as the one presented in [34]. Our theory—under assumptions on the condition number of the objective and the optimal solution—proves convergence when such acceleration is used in factorized gradient descent for matrix sensing. This expands the recent results on the favorable performance of non-convex algorithms over convex methods.

- We provide empirical justification both in synthetic and real-life settings. For the latter, we focus on two applications: **(i)** the task of identifying neuronal activities located at different depths of the brain: the idea is that the observations at the surface of the brain are linear combinations of these neural activities, lowpass filtered and attenuated as per their depths. **(ii)** The task of quantum state tomography (QST) using quantum computing simulators and actual quantum machines [35, 36]: pure quantum states are naturally represented as low-rank density matrices, and the QST becomes prohibitive computationally as the number of qubits of the system increases.

There are remaining open questions. The range of momentum values that comply with our theory is conservative; we also assume problem instances with fairly well-conditioned optimal solutions. Further, while we prove linear convergence when acceleration is used, the same dependence on the condition number(s) is observed as in [34]; whether this can be improved is an open question.

2 Setup

The matrix sensing problem has been studied extensively in the literature; see [37] and references to it. It has numerous applications including, video background subtraction [38, 39], system approximation [40], and identification [41], robust PCA [42, 38], and quantum state tomography [43, 44].

Here, following the path in [45, 46, 30], we consider the matrix sensing problem for square matrices $X \in \mathbb{R}^{n \times n}$, under both low rank and positive semi-definite (PSD) constraints:¹

$$\min_{X \in \mathbb{R}^{n \times n}} f(X) := \frac{1}{2} \|\mathcal{A}(X) - y\|_2^2 \quad \text{subject to } X \succeq 0, \text{rank}(X) \leq r. \quad (1)$$

X is the random variable that lives at the intersection of low-rank and PSD constraints; $y \in \mathbb{R}^m$ is the set of observations; and $\mathcal{A}(\cdot) : \mathbb{R}^{n \times n} \rightarrow \mathbb{R}^m$ is the linear sensing map, where $m \ll n^2$. Common \mathcal{A} is the trace operator where $(\mathcal{A}(X))_i = \text{Tr}(A_i^\top X)$, for symmetric random $A_i \in \mathbb{R}^{n \times n}$.

Pivotal assumption is that \mathcal{A} satisfies the *restricted isometry property*:

Definition 1 (Restricted Isometry Property (RIP) [37]). *A linear operator $\mathcal{A} : \mathbb{R}^{n \times n} \rightarrow \mathbb{R}^m$ satisfies the restricted isometry property on rank- r matrices, with parameter $\delta_r \in (0, 1)$, if the following set of inequalities hold for all rank- r matrices X :*

$$(1 - \delta_r) \cdot \|X\|_F^2 \leq \|\mathcal{A}(X)\|_2^2 \leq (1 + \delta_r) \cdot \|X\|_F^2.$$

A classical way to solve (1) is via the *projected gradient descent*:

$$X_{i+1} = \Pi_{\substack{\text{rank}(\cdot) \leq r, \\ X \succeq 0}} (X_i - \eta \mathcal{A}^\dagger (\mathcal{A}(X_i) - y)). \quad (2)$$

I.e., we refine X_i using the negative gradient, and projecting on the intersection of low-rank and PSD constraints. $\mathcal{A}^\dagger : \mathbb{R}^m \rightarrow \mathbb{R}^{n \times n}$ is the adjoint of \mathcal{A} , defined as $\mathcal{A}(x) = \sum_{i=1}^m x_i A_i$, for $x \in \mathbb{R}^m$.

Recent works focus on the factorized version of the problem, due to time/space complexity savings:²

$$\min_{U \in \mathbb{R}^{n \times r}} \frac{1}{2} \|\mathcal{A}(UU^\top) - y\|_2^2; \quad (3)$$

see also the Related Work section for a subset of references on the subject. Observe that any matrix $X \succeq 0$ with $\text{rank}(X) \leq r$, can be written as $X = UU^\top$, for $U \in \mathbb{R}^{n \times r}$; this re-parameterization encapsulates both constraints in (1) into the objective of (3). This however leads to the non-convex problem formulation above, where gradient descent transforms into:³

$$U_{i+1} = U_i - \eta \nabla f(U_i U_i^\top) \cdot U_i = U_i - \eta \mathcal{A}^\dagger (\mathcal{A}(U_i U_i^\top) - y) \cdot U_i.$$

This algorithm has been studied in [45, 48, 34, 49, 50, 51]. We will refer to the above recursion as the *Procrustes Flow* algorithm, as in [34]. None of the above works have considered momentum acceleration on U . In this work, we will study the accelerated version of Procrustes Flow.

¹The rectangular case can be derived, after proper transformations, using ideas from [47].

²Eqn. (2) includes full eigenvalue decompositions with time complexity $O(n^3)$ and storage $O(n^2)$.

³We assume cases where $\nabla f(\cdot) = \nabla f(\cdot)^\top$. If this does not hold, the theory goes through by carrying around $\nabla f(\cdot) + \nabla f(\cdot)^\top$ instead of just $\nabla f(\cdot)$, after proper scaling.

3 Accelerated Procrustes Flow and Main Results

We consider the following variant of Procrustes flow:

$$U_{i+1} = Z_i - \eta \mathcal{A}^\dagger (\mathcal{A}(Z_i Z_i^\top) - y) \cdot Z_i, \quad Z_{i+1} = U_{i+1} + \mu (U_{i+1} - U_i).$$

Here, Z_i is the auxiliary variable that accumulates the ‘‘momentum’’ of the variable U ; the dimensions are apparent from the context. μ is the momentum parameter that weighs how the previous estimates U_i will be mixed with the current estimate U_{i+1} to generate Z_{i+1} .

The above recursion follows from Nesterov’s accelerated first-order method [2] on convex problems: Briefly, consider the generic convex optimization problem: $\min_{x \in \mathbb{R}^d} g(x)$, where g is a convex function, that satisfies standard Lipschitz gradient continuity assumptions, with Lipschitz constant L . Then, Nesterov’s acceleration follows the recursion: $x_{i+1} = y_i - \frac{1}{L} \nabla g(y_i)$, and $y_{i+1} = x_{i+1} + \mu_i (x_{i+1} - x_i)$, where μ_i follows a specific⁴ rule: $t_0 = 0$, $t_i = \frac{1 + \sqrt{1 + 4t_{i-1}^2}}{2}$, and $\mu_i = \frac{1 - t_i}{t_{i+1}}$. We borrow the momentum formulation as shown above, but we study *how constant μ selections behave in non-convex problem formulations*, such as in (3). We note that the theory and algorithmic configurations in [2] do not trivially generalize to non-convex problems.

Preliminaries. We first need some nomenclature. An important observation on any $X = UU^\top$ factorization is that it is not unique. That is, if there is an optimal solution U^* for (3), one can construct a matrix $R \in \mathbb{R}^{r \times r}$, such that $R^\top R = I$; then, $\hat{U} = U^* R$ is also a solution since $\hat{U} \hat{U}^\top = U^* R \cdot R^\top U^{*\top} = U^* U^{*\top}$. We disambiguate such situations by defining the distance between a pair of matrices as the minimum distance $\|U - U^* R\|_F$, for $R \in \mathbb{R}^{r \times r}$ such that $R^\top R = I$.

The algorithm. The algorithm on the right contains the details of the Accelerated Procrustes Flow. The algorithm requires as input the target rank⁵ r , the number of iterations J , and the momentum parameter μ . For our theory to hold, we make the following selections. **(i)** We set $\mu = 1/1000$; as we state later in the text, this selection is arbitrary and conservative, and different μ choices lead to different requirements in our theory. **(ii)** We use step size:

$$\eta = \frac{1}{4((1 + \delta_{2r}) \|Z_0 Z_0^\top\|_2 + \|\mathcal{A}^\dagger(\mathcal{A}(Z_0 Z_0^\top) - y)\|_2)}, \quad (4)$$

where $Z_0 = (1 + \mu)U_0$. Observe that η remains constant throughout the execution, and requires two top-eigenvalue computations: that of $\|Z_0 Z_0^\top\|_2$ and $\|\mathcal{A}^\dagger(\mathcal{A}(Z_0 Z_0^\top) - y)\|_2$. Our experiments show that this step can be efficiently implemented by any off-the-shelf eigenvalue solver, such as the Power Method or the Lanczos method. **(iii)** The initial point U_0 is either randomly selected [46, 49], or set according to the following Lemma:

Lemma 1 ([53]). *Let U_0 such that $X_0 = U_0 U_0^\top = \Pi_C \left(\frac{-1}{1 + \delta_{2r}} \cdot \nabla f(0) \right)$, where $\Pi_C(\cdot)$ is the projection onto the set of PSD matrices, and $\nabla f(0)$ denotes the gradient evaluated at the all zero matrix. Consider the matrix sensing problem with RIP for some constant $\delta_{2r} \in (0, 1)$. Further, assume the optimum point X^* satisfies $\text{rank}(X^*) = r$. Then, $\exists R \in \mathcal{O}$ such that:*

$$\|U_0 - U^* R\|_F \leq \gamma' \cdot \sigma_r(U^*), \text{ where } \gamma' = \sqrt{\frac{1 - \delta_{2r}}{2(\sqrt{2} - 1)}} \cdot \tau(X^*) \cdot \sqrt{\text{srank}(X^*)}, \tau(X^*) = \frac{\sigma_1(X^*)}{\sigma_r(X^*)}, \text{ and } \text{srank}(X) = \frac{\|X\|_F}{\sigma_1(X)}.$$

Since computing the RIP constants is NP-hard, in practice we compute $X_0 = \Pi_C(-1/\hat{L} \cdot \nabla f(0))$, where $\hat{L} \in (1, 2)$. We do not know *a priori* $\tau(X^*)$ and $\text{srank}(X^*)$ to compute γ' , but they can be approximated depending on the problem at hand; e.g., in the quantum state tomography case, the rank could be $r = 1$ (for pure quantum states), and we know *a priori* that $\tau(X^*) = \text{srank}(X^*) = 1$, by construction. Compared to randomly selecting U_0 , Lemma 1 involves a gradient descent computation and a top- r eigenvalue calculation; while randomly selecting an initial point guarantees convergence [46, 49], Lemma 1 provides the initial conditions for our theory.

Main theorem. The following theorem proves the convergence of accelerated Procrustes Flow under assumptions on μ , the RIP constant δ_{2r} , the condition number of the objective κ (defined below) and that of the optimal solution $\tau(X^*)$, and assuming the

⁴This is probably the most famous sequence of μ values; in his seminal book on convex optimization [52], Nesterov proposes and analyzes other μ sequences that also lead to similar convergence rates.

⁵In this work, we assume we know the target rank *a priori*. For the cases where we undershot the rank, the theory from [47] can be used to extend our theory. We select not to present this case here for the sake of clarity and simplicity.

Input: \mathcal{A} , y , r , and # iterations J .

Set η as in (4), and $\mu = 1/1000$

Set U_0 randomly or according to Lemma 1, and $Z_0 = (1 + \mu)U_0$.

for $i = 0$ to $J - 1$ **do**

$$U_{i+1} = Z_i - \eta \mathcal{A}^\dagger (\mathcal{A}(Z_i Z_i^\top) - y) \cdot Z_i$$

$$Z_{i+1} = U_{i+1} + \mu (U_{i+1} - U_i)$$

end for

Output: $X = U_J U_J^\top$

Figure 1: Accelerated Procrustes Flow

initialization in Lemma 1. We note that such assumptions are needed in order to provide a concrete and qualitative convergence result.

Theorem 1 (Convergence Rate). *Assume that \mathcal{A} satisfies the RIP with constant $\delta_{2r} \leq 1/10$. Let U_0 be such that $\|U_0 - U^*R\|_F \leq \frac{\sigma_r(X^*)^{1/2}}{200\sqrt{\kappa\tau(X^*)}}$, for some $R \in \mathcal{O}$, where $\kappa := \frac{1+\delta_{2r}}{1-\delta_{2r}}$ and $\tau(X) := \frac{\sigma_1(X)}{\sigma_r(X)}$ for rank- r X . Set η according to (4) and the momentum parameter $\mu = 1/1000$. For the noiseless case $y = \mathcal{A}(X^*)$, where X^* is rank- r , Algorithm 1 satisfies:*

$$\|U_{J+1} - U^*R\|_F \leq \frac{|\lambda_1|^{J+1} \cdot \gamma}{|\lambda_1| - |\lambda_2|} \|U_0 - U^*R\|_F, \text{ where } \gamma = 2(\xi(|1+\mu| + |\mu|) + 1) \text{ is constant,} \quad (5)$$

$$\text{for } \xi := e^{-\frac{4}{25\tau(X^*)}}, \mu = 1/1000, \tau(X^*) \leq 3.3209, \text{ and } |\lambda_{1,2}| = \left| \frac{\xi \cdot |1+\mu| \pm \sqrt{\xi^2(1+\mu)^2 + 4\xi|\mu|}}{2} \right| < 1.$$

The above theorem shows that the accelerated Procrustes Flow algorithm converges linearly to the optimal solution in the noiseless case (as long as $|\lambda_{1,2}| < 1$).

Remark 1. *Observe that the contraction constants in (5) depend on $\tau(X^*)$ and κ ;⁶ classic results from convex optimization depend on the $\sqrt{\kappa}$. It remains an open question whether provably acceleration with dependence on at least $\sqrt{\kappa}$ can be achieved using our method. We also note that even the acceleration guarantee for strongly convex and smooth functions does not generalize to all strongly convex and smooth functions [54]. However, acceleration is observed in practice in most cases.*

Remark 2. *Different choices of $(\tau(X^*), \mu, \delta_{2r})$ lead to different dependences between them.*

4 Proof of the main theorem

Notation and preliminaries: The Frobenius and spectral norms of a matrix X are $\|X\|_F$ and $\|X\|_2$, respectively. The inner product between two matrices $X, Y \in \mathbb{R}^{m \times n}$ is given by $\langle X, Y \rangle = \text{Tr}(X^T Y)$. The singular values of X are denoted by $\sigma_i(X)$, $i = 1, \dots, r$. Note $\|X\|_2 = \sigma_1(X)$.

Proof of Theorem 1: We denote $U_+ \equiv U_{i+1}$, $U \equiv U_i$, $U_- \equiv U_{i-1}$ and $Z \equiv Z_i$. Let us start with the following equality. Given that U_0 is close enough the solution U^*R , for some $R \in \mathcal{O}$,⁷ we have:

$$\|U_+ - U^*R\|_F^2 = \|U_+ - Z\|_F^2 + \|Z - U^*R\|_F^2 - 2\langle U_+ - Z, U^*R - Z \rangle$$

The proof focuses on how to bound the last part on the right-hand side. We use the following Lemmata and Corollary; the proofs can be found in the appendix.

Lemma 2. *Let $U \in \mathbb{R}^{n \times r}$, $U_- \in \mathbb{R}^{n \times r}$, and $U^* \in \mathbb{R}^{n \times r}$, such that $\|U - U^*R\|_F \leq \frac{\sigma_r(X^*)^{1/2}}{200\sqrt{\kappa\tau(X^*)}}$ and $\|U_- - U^*R\|_F \leq \frac{\sigma_r(X^*)^{1/2}}{200\sqrt{\kappa\tau(X^*)}}$, where $X^* = U^*U^{*\top}$, and $\kappa := \frac{1+\delta_{2r}}{1-\delta_{2r}} > 1$, for $\delta_{2r} \leq 1/10$, and $\tau(X^*) := \frac{\sigma_1(X^*)}{\sigma_r(X^*)} > 1$. By Lemma 6, the above imply also that: $\|Z - U^*R\|_F \leq (1 + 2|\mu|) \cdot \frac{\sigma_r(X^*)^{1/2}}{200}$. Then, under RIP assumptions, and denoting $\Delta_Z = Z - U^*R$, we have:*

$$\left\langle \mathcal{A}^\dagger(\mathcal{A}(ZZ^\top) - y), \Delta_Z \Delta_Z^\top \right\rangle \geq -\left(\theta \sigma_r(X^*) \|\Delta_Z\|_F^2 + \frac{10.1\beta^2\hat{\eta}(1+2|\mu|)^2}{100\left(1 - \frac{1}{200}(1+2|\mu|)\right)^2} \|\mathcal{A}^\dagger(\mathcal{A}(ZZ^\top) - y) \cdot Z\|_F^2 \right)$$

$$\text{where } \theta = \frac{(1 - \delta_{2r})(1 + (1 + 2|\mu|)\frac{1}{200})^2}{1000} + (1 + \delta_{2r}) \left(2 + (1 + 2|\mu|) \cdot \frac{1}{200} \right) (1 + 2|\mu|) \cdot \frac{1}{200}, \quad \hat{\eta} = \frac{1}{4((1+\delta_r)\|ZZ^\top\|_2 + \|\mathcal{A}^\dagger(\mathcal{A}(ZZ^\top) - y)Q_Z Q_Z^\top\|_2)}, \text{ and } \beta := \frac{1+(1+2|\mu|)\cdot\frac{1}{200}}{1-(1+2|\mu|)\cdot\frac{1}{200}} > 1.$$

Based on the assumptions, we get the following corollary, by substituting μ .

Corollary 1. *Under same assumptions, and assuming $\delta_{2r} \leq 1/10$, $\mu = 1/1000$, Lemma 2 becomes:*

$$\left\langle \mathcal{A}^\dagger(\mathcal{A}(ZZ^\top) - y), \Delta_Z \Delta_Z^\top \right\rangle \geq -\left(\frac{1.4}{100} (1 - \delta_{2r}) \sigma_r(X^*) \|\Delta_Z\|_F^2 + 0.1049 \cdot \|\mathcal{A}^\dagger(\mathcal{A}(ZZ^\top) - y) \cdot Z\|_F^2 \right)$$

Lemma 3. *Under similar assumptions with Lemma 2, the following inequality holds:*

$$\left\langle \mathcal{A}^\dagger(\mathcal{A}(ZZ^\top) - y), ZZ^\top - U^*U^{*\top} \right\rangle \geq 1.1172\eta \left\| \mathcal{A}^\dagger(\mathcal{A}(ZZ^\top) - y) Z \right\|_F^2 + \frac{1-\delta_{2r}}{2} \|U^*U^{*\top} - ZZ^\top\|_F^2$$

⁶This is not obvious from this result, but it is shown in the full proof, where we bound κ using $\delta_{2r} \leq 1/10$

⁷We assume that the initialization condition places the algorithm to a initial point where R remains the same during the execution; *i.e.*, the algorithm moves towards a minimum for a fixed R .

Going back to our original equation, we have:

$$\begin{aligned}
\|U_+ - U^*R\|_F^2 &= \eta^2 \|\mathcal{A}^\dagger (\mathcal{A}(ZZ^\top) - y)\|_F^2 + \|Z - U^*R\|_F^2 \\
&\quad - \eta \langle \mathcal{A}^\dagger (\mathcal{A}(ZZ^\top) - y), ZZ^\top - U^*U^{*\top} \rangle - \eta \langle \mathcal{A}^\dagger (\mathcal{A}(ZZ^\top) - y), \Delta_Z \Delta_Z^\top \rangle \\
&\leq \|U_+ - Z\|_F^2 + \|Z - U^*R\|_F^2 - 1.1172\eta^2 \left\| \mathcal{A}^\dagger (\mathcal{A}(ZZ^\top) - y) Z \right\|_F^2 - \eta \frac{1-\delta_{2r}}{2} \|U^*U^{*\top} - ZZ^\top\|_F^2 \\
&\quad + \eta \left(\theta \sigma_r(X^*) \cdot \|Z - U^*R\|_F^2 + \frac{10.1\beta^2 \hat{\eta}(1+2|\mu|)^2}{100 \left(1 - (1+2|\mu|) \frac{1}{200}\right)^2} \cdot \|\mathcal{A}^\dagger (\mathcal{A}(ZZ^\top) - y) \cdot Z\|_F^2 \right)
\end{aligned}$$

Next, we use the following lemma:

Lemma 4. [34, Lemma 5.4] For any Z, U^* , $\|U^*U^{*\top} - ZZ^\top\|_F^2 \geq 2(\sqrt{2} - 1) \cdot \sigma_r(X^*) \cdot \|Z - U^*R\|_F^2$.

which, in our main recursion, results in:

$$\begin{aligned}
\|U_+ - U^*R\|_F^2 &\leq \left(1 + \frac{10.1\beta^2}{100} \cdot \frac{10}{9} \cdot \frac{(1+2|\mu|)^2}{\left(1 - (1+2|\mu|) \frac{1}{200}\right)^2} - 1.1172 \right) \eta^2 \|\mathcal{A}^\dagger (\mathcal{A}(ZZ^\top) - y) \cdot Z\|_F^2 \\
&\quad + \left(1 + \theta \sigma_r(X^*) - \eta(\sqrt{2} - 1)(1 - \delta_{2r})\sigma_r(X^*) \right) \|Z - U^*R\|_F^2
\end{aligned}$$

which is due to Lemma 7 in the appendix, and due to the definition of U_+ .

Remark 3. The discussion so far holds without any assumption on μ ; nexts, we will set $\mu = 1/1000$; in practice, larger values for μ still lead to accelerated convergence in our experiments, which implies that the proof can be improved for stricter initialization assumptions and different μ values. Different μ values lead to different conditions for the main quantities/assumptions involved.

Assuming $\mu = 1/1000$ and $\delta_{2r} \leq 1/10$, we obtain:

$$\|U_+ - U^*R\|_F^2 \leq \left(1 - \frac{4\eta\sigma_r(X^*)(1-\delta_{2r})}{10} \right) \|Z - U^*R\|_F^2 \quad (6)$$

By Lemma 7, we know that $\eta \geq \frac{100}{102}\eta^*$. Also, $\eta^* = \frac{1}{4(1+\delta_{2r})\|X^*\|_2}$, since $\|\mathcal{A}^\dagger (\mathcal{A}(X^*) - y)\|_2 = 0$, in the noiseless setting. Returning to (8), we have:

$$\|U_+ - U^*R\|_F^2 \leq \left(1 - 0.393 \cdot \frac{(1-\delta_{2r})\sigma_r(X^*)}{(1+\delta_{2r})\sigma_1(X^*)} \right) \|Z - U^*R\|_F^2 = \left(1 - \frac{0.393}{\kappa\tau(X^*)} \right) \|Z - U^*R\|_F^2$$

Taking square root on both sides, we obtain: $\|U_+ - U^*R\|_F \leq \sqrt{1 - \frac{0.393}{\kappa\tau(X^*)}} \|Z - U^*R\|_F$. We know that, for $|x| \leq 1$: $\sqrt{1+x} \leq e^{x/2} \leq \sqrt{1+x+x^2}$. Setting $x = -\frac{0.393}{\kappa\tau(X^*)}$, we have:

$$\|U_+ - U^*R\|_F \leq e^{-\frac{0.393}{2\kappa\tau(X^*)}} \|Z - U^*R\|_F \leq \xi \|Z - U^*R\|_F,$$

where $\xi := e^{-\frac{4}{25\tau(X^*)}}$, and $\kappa = \frac{1+\delta_{2r}}{1-\delta_{2r}} \leq \frac{11}{9}$, assuming $\delta_{2r} \leq 1/10$. Using the definition of Z :

$$\begin{aligned}
\|U_+ - U^*R\|_F &\leq \xi \|U + \mu(U - U_-) - U^*R\|_F = \xi \|U + \mu(U - U_-) - (1 - \mu + \mu)U^*R\|_F \\
&\leq \xi \cdot |1 + \mu| \cdot \|U - U^*R\|_F + \xi \cdot |\mu| \cdot \|U_- - U^*R\|_F
\end{aligned}$$

Define $h(i) = \|U_i - U^*R\|_F$; this leads to the following second-order linear system:

$$h(i+1) \leq \xi \cdot |1 + \mu| \cdot h(i) + \xi \cdot |\mu| \cdot h(i-1).$$

We can convert this into a two-dimensional first-order system, where the variables of the linear system are multi-dimensional. To do this, we define a new state variable $q(i) := h(i+1)$. Using $q(i)$, we define the following 2-dimensional, first-order system:

$$\begin{cases} q(i) - \xi \cdot |1 + \mu| \cdot h(i) - \xi \cdot |\mu| \cdot h(i-1) \leq 0, \\ h(i) \leq q(i-1). \end{cases}$$

This further characterizes the evolution of two state variables, $\{q(i), h(i)\}$:

$$\begin{bmatrix} q(i) \\ h(i) \end{bmatrix} \leq \begin{bmatrix} \xi|1+\mu| & \xi|\mu| \\ 1 & 0 \end{bmatrix} \cdot \begin{bmatrix} q(i-1) \\ h(i-1) \end{bmatrix} \Rightarrow \begin{bmatrix} \|U_{i+1} - U^*R\|_F \\ \|U_i - U^*R\|_F \end{bmatrix} \leq \underbrace{\begin{bmatrix} \xi|1+\mu| & \xi|\mu| \\ 1 & 0 \end{bmatrix}}_{:=A} \cdot \begin{bmatrix} \|U_i - U^*R\|_F \\ \|U_{i-1} - U^*R\|_F \end{bmatrix},$$

where in the last inequality we use the definitions $h(i) = \|U_i - U^*R\|_F$ and $q(i) = h(i+1)$. Observe that the contraction matrix has non-negative values. Unfolding the recursion for J iterations:

$$\begin{bmatrix} \|U_{J+1} - U^*R\|_F \\ \|U_J - U^*R\|_F \end{bmatrix} \leq A^J \cdot \begin{bmatrix} \|U_1 - U^*R\|_F \\ \|U_0 - U^*R\|_F \end{bmatrix}.$$

Define $y(i) = \begin{bmatrix} \|U_{i+1} - U^*R\|_F \\ \|U_i - U^*R\|_F \end{bmatrix}$; then, the above expression becomes $y(J) \leq A^J \cdot y(0)$. A has only non-negative values.

Here, we make the convention that $\|U_{-1} - U^*R\|_F = \|U_0 - U^*R\|_F$, such that $y(-1) = \begin{bmatrix} 1 \\ 1 \end{bmatrix} \cdot \|U_0 - U^*R\|_F$. Re-using Lemma 2 in [22], and the result on the power of 2×2 matrices [55], we obtain:

$$y(J) \leq \frac{\lambda_1^{J+1} - \lambda_2^{J+1}}{\lambda_1 - \lambda_2} \cdot A \cdot y(-1) - \lambda_1 \lambda_2 \frac{\lambda_1^J - \lambda_2^J}{\lambda_1 - \lambda_2} \cdot y(-1).$$

In order to achieve convergence (*i.e.*, the RHS converges to zero), the eigenvalues of A play a crucial role: Both A and $y(-1)$ are constant quantities, and only how fast the quantities $\lambda_1^{J+1} - \lambda_2^{J+1}$ and $\lambda_1^J - \lambda_2^J$ “shrink” matter most. The above suggest that we require $|\lambda_{1,2}| < 1$ for convergence. Under the assumption that $\mu = 1/1000$, results into: $|\lambda_{1,2}| \leq 0.853e^{\frac{1}{\tau(X^*)}} + 0.855e^{\frac{1}{2\tau(X^*)}} - 2 \leq 0$. This is satisfied for any X^* such that: $\tau(X^*) \leq 3.3209$, as already assumed. Using the assumption $|\lambda_{1,2}| < 1$, our main recursion further transforms to:

$$\begin{aligned} y(J) &\stackrel{(i)}{\leq} \frac{|\lambda_1|^{J+1} + |\lambda_2|^{J+1}}{|\lambda_1| - |\lambda_2|} \cdot A \cdot y(-1) + |\lambda_1 \lambda_2| \cdot \frac{|\lambda_1|^J + |\lambda_2|^J}{|\lambda_1| - |\lambda_2|} \cdot y(-1) \\ &\stackrel{(ii)}{\leq} \frac{2|\lambda_1|^{J+1}}{|\lambda_1| - |\lambda_2|} \cdot A \cdot y(-1) + |\lambda_1| \cdot \frac{2|\lambda_1|^J}{|\lambda_1| - |\lambda_2|} \cdot y(-1) \end{aligned}$$

where (i) is due to $A \cdot y(-1)$ and $y(-1)$ being positive quantities, and (ii) is due to $1 > |\lambda_1| > |\lambda_2|$, w.l.o.g. Focusing on the first entry of $y(J)$, we get:

$$\|U_{J+1} - U^*R\|_F \leq \frac{2|\lambda_1|^{J+1}}{|\lambda_1| - |\lambda_2|} \cdot \left(e^{-\frac{4}{25\tau(X^*)}} \cdot (1 + \mu + |\mu|) + 1 \right) \cdot \|U_0 - U^*R\|_F$$

This suggests that, as long as $|\lambda_{1,2}| < 1$, the first term on the right-hand side “shrinks” exponentially with rate $|\lambda_1|^{J+1}$, but also depends (inverse proportionally) on the spectral gap $|\lambda_1| - |\lambda_2|$.

5 Related Work

Matrix sensing has been first provably studied in the convex setting using nuclear norm minimization [37, 56, 41]. Non-convex approaches involving rank-constraints have been proposed in [57, 58, 21]. In both cases, the algorithms involve a full or at least a truncated SVD per iteration.

General low-rank minimization problems have been recently studied from the non-convex factorized formulation, due to computational and space complexity advantages [59, 60, 61, 62, 49, 63, 45, 46, 47, 50, 51, 53]. The factorized version was popularized in solving semi-definite programming (SDP) [64].

Using factorization in matrix sensing, the *Procrustes Flow* approach was studied in [34, 48], with certain initializations techniques, different from the current work: we rely on a unique top- r SVD computation, instead of multiple ones. Finally, [45] proposed the Factored Gradient Descent (FGD) algorithm with a novel step size selection, and presented convergence rates for the algorithm for general convex functions; we extend their work using acceleration in matrix sensing.

6 Neuron activity recovery from μ ECoG

A major hurdle in understanding the human brain is inferring the activities of individual neurons from meso-scales cortical surface electrical potentials, recorded by electrocorticography (ECoG). Here, we present a novel application for low rank matrix sensing to recover single-neuron activities from a single μ ECoG electrode. We simulated recordings of stimulus evoked cortical surface electrical potentials using a single μ ECoG electrode over a short time period; we observe a vector of electrical potentials $y \in \mathbb{R}^m$ for m time instances. The membrane potentials of a set of neurons over this time period which we wish to recover can be viewed as a matrix $X \in \mathbb{R}^{n \times m}$, where each row is the membrane potential for a neuron at m time instances. This matrix will be low rank since neurons are excited for a very short period, after the onset of the stimuli.

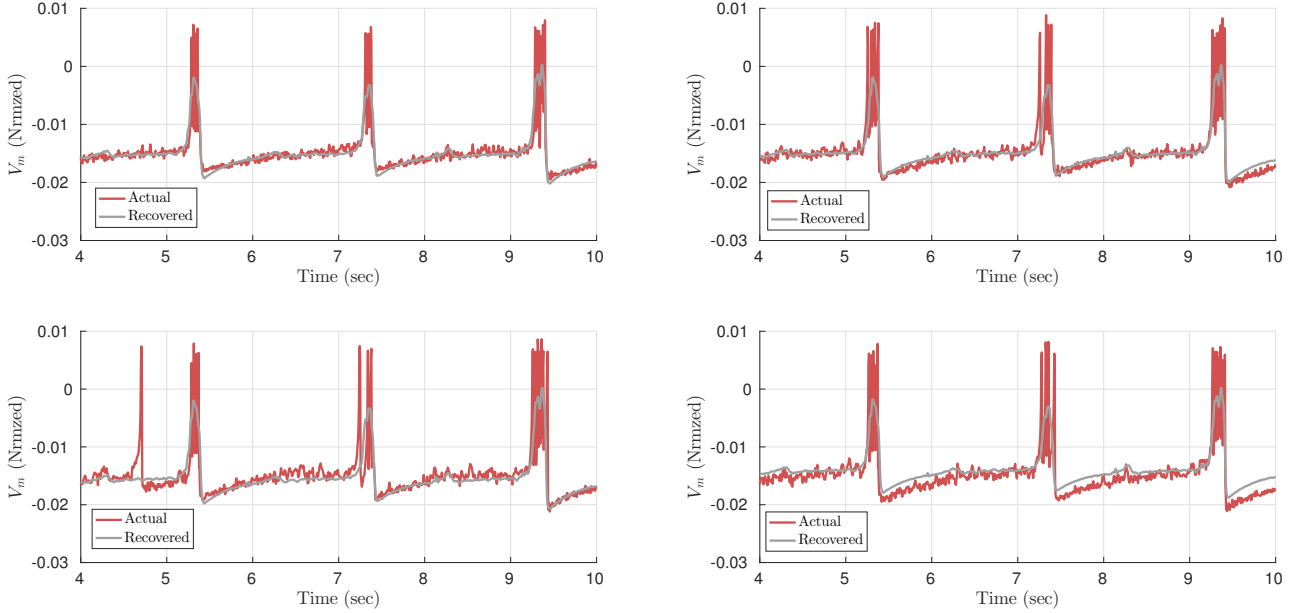


Figure 2: Neuronal activity recovery: The actual membrane potentials between 4 to 10 secs of simulation and the recovered potentials for four neurons at different distances.

Based on [65], the activity of neurons are low-pass filtered with a cut-off frequency that depends on the distance of the neuron from the surface [$f_c(d)$], amplitude attenuated according to distance [$A(d)$], producing distance dependent extracellular potentials. The μ ECoG recordings y are the summation of these extracellular potentials. The distance dependent amplitude attenuation and cut-off frequency are given by: $A(d) = \frac{1}{d^\alpha}$ and $f_c(d) = \frac{f_{\max}}{d^\alpha}$, $\alpha = \Delta_1$, for $d < h$ and $\alpha = \Delta_2$ for $d \geq h$. Here h is in units of distance from the brain surface to allow for potential piecewise linear.

We can view the μ ECoG recordings y as linear mapping of the membrane potentials of the neurons: $y = \mathcal{A}(X) = \mathbf{A}\text{vec}(X)$, where $\mathbf{A} \in \mathbb{R}^{m \times nm}$ is a banded matrix which accounts for the distance dependent lowpass filtering and amplitude attenuation of the membrane potentials of neurons. Experiments can lead to hours of μ ECoG recordings (m in millions) and neural activities are defined for $n \approx 31000$ neurons in a neocortical volume, see; [66]. Hence, the use of factorized algorithms, and their accelerations, in these applications is necessary.

Here, we use the low-rank matrix sensing model and a rectangular version of accelerated Procrustes flow (*i.e.*, X as UV^\top) to recover the neuronal activity X ; we defer the reader to [47, Section 3.1] for an equivalent transformation between rectangular and square matrix factorizations. In Figure 2, we present results for recovering neuronal potentials from a 20secs ($m = 4200$) μ ECoG simulation y ; see also the appendix. We note that our model recovers the potentials of individual neurons very well, though not at single-action potential resolution. *To the best of our knowledge, such recovery results have not been demonstrated before*: they open the possibility of recovering the activities of individual neurons (the ‘microscopic units’) from meso-scale signals recorded in humans (ECoG).

7 Quantum state tomography (QST)

We focus on QST of a low-rank q -qubit state, X^* , from measuring expectation values of q -qubit Pauli observables $\{A_i\}_{i=1}^m$. In our notation, we denote by $y \in \mathbb{R}^m$ the measurement vector with elements $y_i = \text{Tr}(A_i \cdot X^*) + e_i$, $i = 1, \dots, m$, for some measurement error e_i . For brevity, we denote $\mathcal{A} : \mathbb{C}^{2^q \times 2^q} \rightarrow \mathbb{R}^m$ as the linear ‘sensing’ map, such that $(\mathcal{A}(X))_i = \text{Tr}(A_i \cdot X)$, for $i = 1, \dots, m$. The specific realization of Pauli matrices is described in Section 14 in the appendix.

We report results for the case of $q = 6$ qubits, *i.e.*, $n = 2^q = 64$; higher dimension experiments are left for future work. We design X^* as a pure, rank-1 density matrix, such that $X \succeq 0$. More details on how we construct X^* are provided in Section 14 in the appendix. We use the IBM Quantum Information Software Kit (QISKit) [67] to complete the simulations. We generate y according to the above, where $m = \lceil 0.6 \cdot n^2 \rceil$. We test the behavior of our algorithm for $\mu \in \{0, 1/8, 1/4, 1/3, 3/4\}$ values; $\mu = 0$ corresponds to the algorithm in [34, 45]. We run each QST realization 10 times.

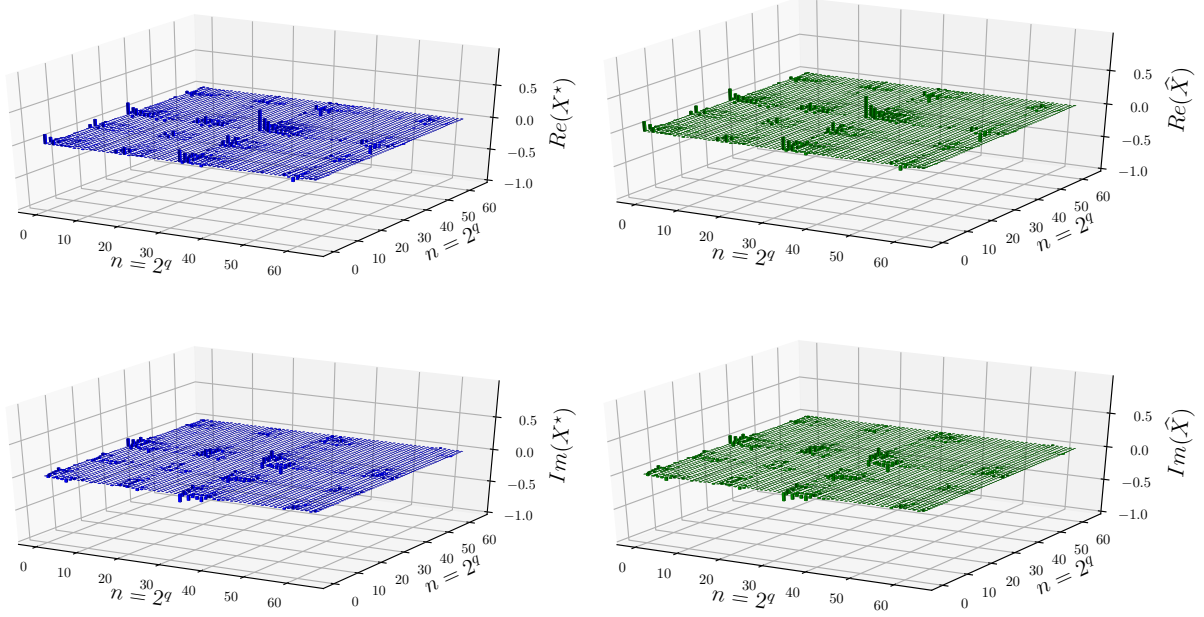


Figure 3: Random rank-1 X^* : *Left panel*: Real and imaginary parts of X^* ; *Right panel*: Reconstructed \hat{X} (real and imaginary parts) for $\mu = 3/4$.

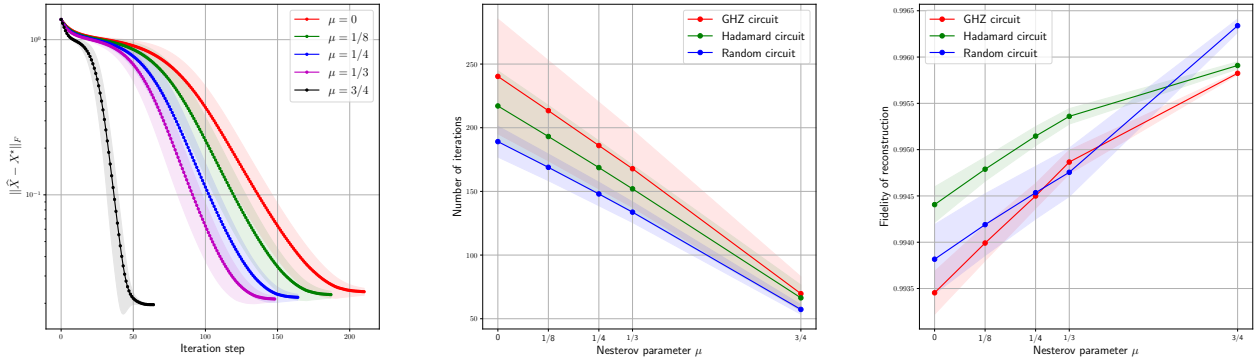


Figure 4: *Left panel*: $\|\hat{X} - X^*\|_F$ vs. # of iterations for different μ ; *Middle panel*: # of iterations to reach `reltol` vs. μ and for different circuits (X^*); *Right panel*: Fidelity of \hat{X} , defined as $\text{Tr}(\sqrt{\sqrt{X^*}\hat{X}\sqrt{X^*}})^2$, vs. μ parameters and for different circuits (X^*). Shaded area denotes standard deviation around the mean over repeated runs in all cases.

Figure 3 shows the complex representation of (i) the target X^* (Left panel), and (ii) its reconstruction \hat{X} (Right panel). X^* is generated as a random rank-1, PSD matrix. We use Algorithm 1 for $\mu = 3/4$. We observe that X^* and \hat{X} are indistinguishable: our scheme succeeds in reproducing the finer details in the density matrix structure.

Figure 4 summarizes the performance of our proposal on different X^* (named circuits in quantum information), and for different μ values. Left panel shows the evolution of the distance $\|\hat{X} - X^*\|_F$ across iterations, featuring a steep dive to convergence for the largest value of μ we tested. Center panel clearly summarizes the acceleration benefits of μ parameter: the # of iterations to reach `reltol` = 5×10^{-4} decreases roughly $\times 3$, as we increase μ ; this behavior is consistent across all our 3 test quantum circuits. Finally, on the right, we see larger μ 's not only accelerate, but also slightly improve the reconstruction quality, in terms of the fidelity metric, roughly defined as the inner product of target and converged states; fidelity equal to one implies that $\hat{X} = X^*$.

References

- [1] B. Polyak. Some methods of speeding up the convergence of iteration methods. *USSR Computational Mathematics and Mathematical Physics*, 4(5):1–17, 1964.
- [2] Y. Nesterov. A method of solving a convex programming problem with convergence rate $O(\frac{1}{k^2})$. In *Soviet Mathematics Doklady*, volume 27, pages 372–376, 1983.
- [3] M. Moreira and E. Fiesler. Neural networks with adaptive learning rate and momentum terms. Technical report, Idiap, 1995.
- [4] I. Sutskever, J. Martens, G. Dahl, and G. Hinton. On the importance of initialization and momentum in deep learning. In *International conference on machine learning*, pages 1139–1147, 2013.
- [5] J. Tompson, A. Jain, Y. LeCun, and C. Bregler. Joint training of a convolutional network and a graphical model for human pose estimation. In *Advances in neural information processing systems*, pages 1799–1807, 2014.
- [6] X. Zhang, J. Zhao, and Y. LeCun. Character-level convolutional networks for text classification. In *Advances in neural information processing systems*, pages 649–657, 2015.
- [7] C. Szegedy, E. Liu, Y. Jia, P. Sermanet, S. Reed, D. Anguelov, D. Erhan, V. Vanhoucke, and A. Rabinovich. Going deeper with convolutions. *Cvpr*, 2015.
- [8] K. Greff, R. Srivastava, J. Koutník, B. Steunebrink, and J. Schmidhuber. LSTM: A search space odyssey. *IEEE transactions on neural networks and learning systems*, 28(10):2222–2232, 2017.
- [9] D. Kingma and J. Ba. Adam: A method for stochastic optimization. *arXiv preprint arXiv:1412.6980*, 2014.
- [10] M. Zeiler. ADADELTA: an adaptive learning rate method. *arXiv preprint arXiv:1212.5701*, 2012.
- [11] T. Tieleman and G. Hinton. Lecture 6.5-RMSProp: Divide the gradient by a running average of its recent magnitude. *COURSERA: Neural networks for machine learning*, 4(2):26–31, 2012.
- [12] T. Dozat. Incorporating Nesterov momentum into Adam. 2016.
- [13] A. Beck and M. Teboulle. A fast iterative shrinkage-thresholding algorithm for linear inverse problems. *SIAM journal on imaging sciences*, 2(1):183–202, 2009.
- [14] A. Chambolle and T. Pock. A first-order primal-dual algorithm for convex problems with applications to imaging. *Journal of mathematical imaging and vision*, 40(1):120–145, 2011.
- [15] S. Becker, J. Bobin, and E. Candès. NESTA: A fast and accurate first-order method for sparse recovery. *SIAM Journal on Imaging Sciences*, 4(1):1–39, 2011.
- [16] M. Afonso, J. Bioucas-Dias, and M. Figueiredo. Fast image recovery using variable splitting and constrained optimization. *IEEE transactions on image processing*, 19(9):2345–2356, 2010.
- [17] B. O’Donoghue and E. Candès. Adaptive restart for accelerated gradient schemes. *Foundations of computational mathematics*, 15(3):715–732, 2015.
- [18] S. Bubeck, Y. T. Lee, and M. Singh. A geometric alternative to Nesterov’s accelerated gradient descent. *arXiv preprint arXiv:1506.08187*, 2015.
- [19] G. Goh. Why momentum really works. *Distill*, 2017.
- [20] A. Kyrillidis and V. Cevher. Recipes on hard thresholding methods. In *Computational Advances in Multi-Sensor Adaptive Processing (CAMSAP), 2011 4th IEEE International Workshop on*, pages 353–356. IEEE, 2011.
- [21] A. Kyrillidis and V. Cevher. Matrix recipes for hard thresholding methods. *Journal of mathematical imaging and vision*, 48(2):235–265, 2014.
- [22] R. Khanna and A. Kyrillidis. IHT dies hard: Provable accelerated iterative hard thresholding. *arXiv preprint arXiv:1712.09379*, 2017.
- [23] S. Ghadimi and G. Lan. Stochastic first-and zeroth-order methods for nonconvex stochastic programming. *SIAM Journal on Optimization*, 23(4):2341–2368, 2013.
- [24] J. Lee, M. Simchowitz, M. Jordan, and B. Recht. Gradient descent only converges to minimizers. In *Conference on Learning Theory*, pages 1246–1257, 2016.
- [25] A. Anandkumar and R. Ge. Efficient approaches for escaping higher order saddle points in non-convex optimization. In *Conference on Learning Theory*, pages 81–102, 2016.
- [26] Y. Carmon, J. Duchi, O. Hinder, and A. Sidford. Accelerated methods for non-convex optimization. *arXiv preprint arXiv:1611.00756*, 2016.

- [27] N. Agarwal, Z. Allen-Zhu, B. Bullins, E. Hazan, and T. Ma. Finding approximate local minima for nonconvex optimization in linear time. *arXiv preprint arXiv:1611.01146*, 2016.
- [28] Z. Allen-Zhu. Natasha 2: Faster non-convex optimization than SGD. *arXiv preprint arXiv:1708.08694*, 2017.
- [29] S. Du, J. Lee, Y. Tian, B. Póczos, and A. Singh. Gradient descent learns one-hidden-layer CNN: Don't be afraid of spurious local minima. *arXiv preprint arXiv:1712.00779*, 2017.
- [30] Y. Li, T. Ma, and H. Zhang. Algorithmic regularization in over-parameterized matrix recovery. *arXiv preprint arXiv:1712.09203*, 2017.
- [31] P. Baldi and K. Hornik. Neural networks and principal component analysis: Learning from examples without local minima. *Neural networks*, 2(1):53–58, 1989.
- [32] D. Boob and G. Lan. Theoretical properties of the global optimizer of two layer neural network. *arXiv preprint arXiv:1710.11241*, 2017.
- [33] I. Safran and O. Shamir. Spurious local minima are common in two-layer ReLU neural networks. *arXiv preprint arXiv:1712.08968*, 2017.
- [34] S. Tu, R. Boczar, M. Simchowitz, M. Soltanolkotabi, and B. Recht. Low-rank solutions of linear matrix equations via Procrustes flow. In *Proceedings of the 33rd International Conference on International Conference on Machine Learning-Volume 48*, pages 964–973. JMLR. org, 2016.
- [35] IBM-Q: Quantum Computing Research. <https://www.research.ibm.com/ibm-q/>.
- [36] C. Wood and John Smolin. A C++ quantum circuit simulator with realistic noise.
- [37] Benjamin Recht, Maryam Fazel, and Pablo A Parrilo. Guaranteed minimum-rank solutions of linear matrix equations via nuclear norm minimization. *SIAM review*, 52(3):471–501, 2010.
- [38] Emmanuel J Candès, Xiaodong Li, Yi Ma, and John Wright. Robust principal component analysis? *Journal of the ACM (JACM)*, 58(3):11, 2011.
- [39] Andrew E Waters, Aswin C Sankaranarayanan, and Richard Baraniuk. Sparcs: Recovering low-rank and sparse matrices from compressive measurements. In *Advances in neural information processing systems*, pages 1089–1097, 2011.
- [40] Maryam Fazel, Haitham Hindi, and Stephen P Boyd. A rank minimization heuristic with application to minimum order system approximation. In *American Control Conference, 2001. Proceedings of the 2001*, volume 6, pages 4734–4739. IEEE, 2001.
- [41] Zhang Liu and Lieven Vandenberghe. Interior-point method for nuclear norm approximation with application to system identification. *SIAM Journal on Matrix Analysis and Applications*, 31(3):1235–1256, 2009.
- [42] Venkat Chandrasekaran, Sujay Sanghavi, Pablo A Parrilo, and Alan S Willsky. Sparse and low-rank matrix decompositions. *IFAC Proceedings Volumes*, 42(10):1493–1498, 2009.
- [43] Scott Aaronson. The learnability of quantum states. In *Proceedings of the Royal Society of London A: Mathematical, Physical and Engineering Sciences*, volume 463, pages 3089–3114. The Royal Society, 2007.
- [44] Steven T Flammia, David Gross, Yi-Kai Liu, and Jens Eisert. Quantum tomography via compressed sensing: error bounds, sample complexity and efficient estimators. *New Journal of Physics*, 14(9):095022, 2012.
- [45] Srinadh Bhojanapalli, Anastasios Kyrillidis, and Sujay Sanghavi. Dropping convexity for faster semi-definite optimization. In *Conference on Learning Theory*, pages 530–582, 2016.
- [46] Srinadh Bhojanapalli, Behnam Neyshabur, and Nati Srebro. Global optimality of local search for low rank matrix recovery. In *Advances in Neural Information Processing Systems*, pages 3873–3881, 2016.
- [47] Dohyung Park, Anastasios Kyrillidis, Constantine Caramanis, and Sujay Sanghavi. Finding low-rank solutions to matrix problems, efficiently and provably. *arXiv preprint arXiv:1606.03168*, 2016.
- [48] Qinqing Zheng and John Lafferty. A convergent gradient descent algorithm for rank minimization and semidefinite programming from random linear measurements. In *Advances in Neural Information Processing Systems*, pages 109–117, 2015.
- [49] Dohyung Park, Anastasios Kyrillidis, Constantine Caramanis, and Sujay Sanghavi. Non-square matrix sensing without spurious local minima via the burer-monteiro approach. *arXiv preprint arXiv:1609.03240*, 2016.
- [50] Rong Ge, Chi Jin, and Yi Zheng. No spurious local minima in nonconvex low rank problems: A unified geometric analysis. *arXiv preprint arXiv:1704.00708*, 2017.
- [51] Ya-Ping Hsieh, Yu-Chun Kao, Rabeeh Karimi Mahabadi, Yurtsever Alp, Anastasios Kyrillidis, and Volkan Cevher. A non-euclidean gradient descent framework for non-convex matrix factorization. Technical report, Institute of Electrical and Electronics Engineers, 2017.

- [52] Y. Nesterov. *Introductory lectures on convex optimization: A basic course*, volume 87. 2013.
- [53] A. Kyriillidis, A. Kalev, D. Park, S. Bhojanapalli, C. Caramanis, and S. Sanghavi. Provable quantum state tomography via non-convex methods. *arXiv preprint arXiv:1711.02524*, 2017.
- [54] L. Lessard, B. Recht, and A. Packard. Analysis and design of optimization algorithms via integral quadratic constraints. *SIAM Journal on Optimization*, 26(1):57–95, 2016.
- [55] K. Williams. The n -th power of a 2×2 matrix. *Mathematics Magazine*, 65(5):336–336, 1992.
- [56] Kiryung Lee and Yoram Bresler. Guaranteed minimum rank approximation from linear observations by nuclear norm minimization with an ellipsoidal constraint. *arXiv preprint arXiv:0903.4742*, 2009.
- [57] Prateek Jain, Raghu Meka, and Inderjit S Dhillon. Guaranteed rank minimization via singular value projection. In *Advances in Neural Information Processing Systems*, pages 937–945, 2010.
- [58] Kiryung Lee and Yoram Bresler. Admira: Atomic decomposition for minimum rank approximation. *IEEE Transactions on Information Theory*, 56(9):4402–4416, 2010.
- [59] Prateek Jain and Inderjit S Dhillon. Provable inductive matrix completion. *arXiv preprint arXiv:1306.0626*, 2013.
- [60] Yudong Chen and Martin J Wainwright. Fast low-rank estimation by projected gradient descent: General statistical and algorithmic guarantees. *arXiv preprint arXiv:1509.03025*, 2015.
- [61] Tuo Zhao, Zhaoran Wang, and Han Liu. A nonconvex optimization framework for low rank matrix estimation. In *Advances in Neural Information Processing Systems*, pages 559–567, 2015.
- [62] Dohyung Park, Anastasios Kyriillidis, Srinadh Bhojanapalli, Constantine Caramanis, and Sujay Sanghavi. Provable burer-monteiro factorization for a class of norm-constrained matrix problems. *arXiv preprint arXiv:1606.01316*, 2016.
- [63] Ruoyu Sun and Zhi-Quan Luo. Guaranteed matrix completion via non-convex factorization. *IEEE Transactions on Information Theory*, 62(11):6535–6579, 2016.
- [64] Samuel Burer and Renato DC Monteiro. A nonlinear programming algorithm for solving semidefinite programs via low-rank factorization. *Mathematical Programming*, 95(2):329–357, 2003.
- [65] K.E. Bouchard, M.E. Dougherty, P. Ledochowitsch, A. Yazdan-Shahmorad, L Muller, E.A.K. Philips, A. Hasenstaub, P.N. Sabes, C.E. Schreiner, M.M. Maharbiz, and E.F Chang. Structure and origin of distinct high-frequency components in evoked cortical surface electrical potentials. *Submitted*, 2018.
- [66] Henry Markram, Eilif Muller, Srikanth Ramaswamy, Michael W Reimann, Marwan Abdellah, Carlos Aguado Sanchez, Anastasia Ailamaki, Lidia Alonso-Nanclares, Nicolas Antille, Selim Arsever, et al. Reconstruction and simulation of neocortical microcircuitry. *Cell*, 163(2):456–492, 2015.
- [67] QISKit Development Team. Qiskit.
- [68] R. Horn and Ch. Johnson. *Matrix analysis*. Cambridge university press, 1990.
- [69] L. Mirsky. A trace inequality of John von Neumann. *Monatshefte für mathematik*, 79(4):303–306, 1975.
- [70] D. Gross, Y.-K. Liu, S. Flammia, S. Becker, and J. Eisert. Quantum state tomography via compressed sensing. *Physical review letters*, 105(15):150401, 2010.
- [71] Y.-K. Liu. Universal low-rank matrix recovery from Pauli measurements. In *Advances in Neural Information Processing Systems*, pages 1638–1646, 2011.

8 Supporting lemmata

In this section, we present a series of lemmata, used for the main result of the paper.

Lemma 5. Let $U \in \mathbb{R}^{n \times r}$ and $U^* \in \mathbb{R}^{n \times r}$, such that $\|U - U^*R\|_F \leq \frac{\sigma_r(X^*)^{1/2}}{200\sqrt{\kappa\tau(X^*)}}$, where $X^* = U^*U^{*\top}$, $\kappa := \frac{1+\delta_{2r}}{1-\delta_{2r}} > 1$, for $\delta_{2r} \leq \frac{1}{10}$, and $\tau(X^*) := \frac{\sigma_1(X^*)}{\sigma_r(X^*)} > 1$. Then:

$$\begin{aligned}\sigma_1(X^*)^{1/2} \left(1 - \frac{1}{200}\right) &\leq \sigma_1(U) \leq \sigma_1(X^*)^{1/2} \left(1 + \frac{1}{200}\right) \\ \sigma_r(X^*)^{1/2} \left(1 - \frac{1}{200}\right) &\leq \sigma_r(U) \leq \sigma_r(X^*)^{1/2} \left(1 + \frac{1}{200}\right)\end{aligned}$$

Proof. By the fact $\|\cdot\|_2 \leq \|\cdot\|_F$ and using the Weyl's inequality for perturbation of singular values [68, Theorem 3.3.16], we have:

$$|\sigma_i(U) - \sigma_i(U^*)| \leq \frac{\sigma_r(X^*)^{1/2}}{200\sqrt{\kappa\tau(X^*)}} \leq \frac{\sigma_r(X^*)^{1/2}}{200}, \quad 1 \leq i \leq r.$$

Then,

$$\begin{aligned}-\frac{\sigma_r(X^*)^{1/2}}{200} &\leq \sigma_1(U) - \sigma_1(U^*) \leq \frac{\sigma_r(X^*)^{1/2}}{200} \Rightarrow \\ \sigma_1(X^*)^{1/2} - \frac{\sigma_r(X^*)^{1/2}}{200} &\leq \sigma_1(U) \leq \sigma_1(X^*)^{1/2} + \frac{\sigma_r(X^*)^{1/2}}{200} \Rightarrow \\ \sigma_1(X^*)^{1/2} \left(1 - \frac{1}{200}\right) &\leq \sigma_1(U) \leq \sigma_1(X^*)^{1/2} \left(1 + \frac{1}{200}\right)\end{aligned}$$

Similarly:

$$\begin{aligned}-\frac{\sigma_r(X^*)^{1/2}}{200} &\leq \sigma_r(U) - \sigma_r(U^*) \leq \frac{\sigma_r(X^*)^{1/2}}{200} \Rightarrow \\ \sigma_r(X^*)^{1/2} - \frac{\sigma_r(X^*)^{1/2}}{200} &\leq \sigma_r(U) \leq \sigma_r(X^*)^{1/2} + \frac{\sigma_r(X^*)^{1/2}}{200} \Rightarrow \\ \sigma_r(X^*)^{1/2} \left(1 - \frac{1}{200}\right) &\leq \sigma_r(U) \leq \sigma_r(X^*)^{1/2} \left(1 + \frac{1}{200}\right)\end{aligned}$$

In the above, we used the fact that $\sigma_i(U^*) = \sigma_i(X^*)^{1/2}$, for all i , and the fact that $\sigma_i(X^*)^{1/2} \geq \sigma_j(X^*)^{1/2}$, for $i \leq j$. \square

Corollary 2. Let $Z \in \mathbb{R}^{n \times r}$ and $U^* \in \mathbb{R}^{n \times r}$, such that $\|Z - U^*R\|_F \leq (1 + 2|\mu|) \cdot \frac{\sigma_r(X^*)^{1/2}}{200}$, and $X^* = U^*U^{*\top}$. Then:

$$\begin{aligned}\sigma_1(X^*)^{1/2} \left(1 - (1 + 2|\mu|) \frac{1}{200}\right) &\leq \sigma_1(Z) \leq \sigma_1(X^*)^{1/2} \left(1 + (1 + 2|\mu|) \frac{1}{200}\right) \\ \sigma_r(X^*)^{1/2} \left(1 - (1 + 2|\mu|) \frac{1}{200}\right) &\leq \sigma_r(Z) \leq \sigma_r(X^*)^{1/2} \left(1 + (1 + 2|\mu|) \frac{1}{200}\right).\end{aligned}$$

For the special case where $\mu = \frac{1}{1000}$, we get:

$$\begin{aligned}0.99499 \cdot \sigma_1(X^*)^{1/2} &\leq \sigma_1(Z) \leq 1.005 \cdot \sigma_1(X^*)^{1/2} \\ 0.99499 \cdot \sigma_r(X^*)^{1/2} &\leq \sigma_r(Z) \leq 1.005 \cdot \sigma_r(X^*)^{1/2}.\end{aligned}$$

Proof. The proof follows similar motions as in Lemma 5. \square

Corollary 3. Under the same assumptions of Lemma 5 and Corollary 2, and assuming $\mu = \frac{1}{1000}$, we have:

$$\begin{aligned}\frac{99}{100} \cdot \|X^*\|_2 &\leq \|ZZ^\top\|_2 \leq \frac{101}{100} \cdot \|X^*\|_2 \\ \frac{99}{100} \cdot \|X^*\|_2 &\leq \|Z_0Z_0^\top\|_2 \leq \frac{101}{100} \cdot \|X^*\|_2\end{aligned}$$

and

$$\frac{99}{101} \cdot \|Z_0Z_0^\top\|_2 \leq \|ZZ^\top\|_2 \leq \frac{101}{99} \cdot \|Z_0Z_0^\top\|_2$$

Proof. The proof is easily derived based on the quantities from Lemma 5 and Corollary 2. \square

Lemma 6. Let $U \in \mathbb{R}^{n \times r}$, $U_- \in \mathbb{R}^{n \times r}$, and $U^* \in \mathbb{R}^{n \times r}$, such that $\|U - U^*R\|_F \leq \frac{\sigma_r(X^*)^{1/2}}{200\sqrt{\kappa\tau(X^*)}}$ and $\|U_- - U^*R\|_F \leq \frac{\sigma_r(X^*)^{1/2}}{200\sqrt{\kappa\tau(X^*)}}$, where $X^* = U^*U^{*\top}$, and $\kappa := \frac{1+\delta_{2r}}{1-\delta_{2r}} > 1$, for $\delta_{2r} \leq \frac{1}{10}$, and $\tau(X^*) := \frac{\sigma_1(X^*)}{\sigma_r(X^*)} > 1$. Then,

$$\|Z - U^*R\|_F \leq (|1 + \mu| + |\mu|) \cdot \frac{\sigma_r(X^*)^{1/2}}{200\sqrt{\kappa\tau(X^*)}} \leq (1 + 2|\mu|) \cdot \frac{\sigma_r(X^*)^{1/2}}{200}.$$

Assuming $\mu = \frac{1}{1000}$, the above expression simplifies into:

$$\|Z - U^*R\|_F \leq \left(1 + \frac{2}{1000}\right) \cdot \frac{\sigma_r(X^*)^{1/2}}{200} \leq 0.00501 \cdot \sigma_r(X^*)^{1/2}$$

Proof. By definition of the distance function:

$$\begin{aligned}
\|Z - U^*R\|_F &= \|Z - U^*R\|_F = \|U + \tau(U - U_-) - U^*R\|_F \\
&= \|U + \tau(U - U_-) - (1 - \tau + \tau)U^*R\|_F \\
&\leq |1 + \mu| \cdot \|U - U^*R\|_F + |\mu| \cdot \|U_- - U^*R\|_F \\
&\leq (|1 + \mu| + |\mu|) \cdot \frac{\sigma_r(X^*)^{1/2}}{200\sqrt{\kappa\tau(X^*)}} \\
&\leq (1 + 2|\mu|) \cdot \frac{\sigma_r(X^*)^{1/2}}{200}.
\end{aligned}$$

Using $\mu = \frac{1}{1000}$, we get the additional result. \square

Corollary 4. Let $Z \in \mathbb{R}^{n \times r}$ and $U^* \in \mathbb{R}^{n \times r}$, such that $\|Z - U^*R\|_F \leq (1 + 2|\mu|) \cdot \frac{\sigma_r(X^*)^{1/2}}{200}$, and $X^* = U^*U^{*\top}$. Define $\tau(W) = \frac{\sigma_1(W)}{\sigma_r(W)}$. Then:

$$\tau(ZZ^\top) \leq \beta^2 \tau(X^*),$$

where $\beta := \frac{1+(1+2|\mu|) \cdot \frac{1}{200}}{1-(1+2|\mu|) \cdot \frac{1}{200}} > 1$. In the special case where $\mu = \frac{1}{1000}$, we get $\beta = 1.0121$.

Proof. The proof uses the definition of the condition number $\tau(\cdot)$ and the results from Lemma 5 and and Corollary 2. \square

Lemma 7. Consider the following three step sizes:

$$\begin{aligned}
\eta &= \frac{1}{4((1 + \delta_{2r})\|Z_0Z_0^\top\|_2 + \|\mathcal{A}^\dagger(\mathcal{A}(Z_0Z_0^\top) - y)\|_2)} \\
\hat{\eta} &= \frac{1}{4((1 + \delta_{2r})\|ZZ^\top\|_2 + \|\mathcal{A}^\dagger(\mathcal{A}(ZZ^\top) - y)Q_ZQ_Z^\top\|_2)} \\
\eta^* &= \frac{1}{4((1 + \delta_{2r})\|X^{*\top}\|_2 + \|\mathcal{A}^\dagger(\mathcal{A}(X^*) - y)\|_2)}.
\end{aligned}$$

Here, $Z_0 \in \mathbb{R}^{n \times r}$ is the initial point, $Z \in \mathbb{R}^{n \times r}$ is the current point, and $X^* \in \mathbb{R}^{n \times n}$ is the optimal solution. Then, under the assumptions that $\text{DIST}(U, U^*) \leq \frac{\sigma_r(X^*)^{1/2}}{200\sqrt{\kappa\tau(X^*)}}$, and $\text{DIST}(Z, U^*) \leq (1 + 2|\mu|) \cdot \frac{\sigma_r(X^*)^{1/2}}{200\sqrt{\kappa\tau(X^*)}}$, and assuming $\mu = \frac{1}{1000}$, we have:

$$\frac{10}{9}\eta \geq \hat{\eta} \geq \frac{10}{10.5}\eta, \quad \text{and} \quad \frac{100}{102}\eta^* \leq \eta \leq \frac{102}{100}\eta^*$$

Proof. The assumptions of the lemma are identical to that of Corollary 3. Thus, we have: $\frac{99}{100} \cdot \|U^*\|_2^2 \leq \|Z\|_2^2 \leq \frac{101}{100} \cdot \|U^*\|_2^2$, $\frac{99}{100} \cdot \|U^*\|_2^2 \leq \|Z_0\|_2^2 \leq \frac{101}{100} \cdot \|U^*\|_2^2$, and $\frac{99}{101} \cdot \|Z_0\|_2^2 \leq \|Z\|_2^2 \leq \frac{101}{99} \cdot \|Z_0\|_2^2$. We focus on the inequality $\hat{\eta} \geq \frac{10}{10.5}\eta$. Observe that:

$$\begin{aligned}
\|\mathcal{A}^\dagger(\mathcal{A}(ZZ^\top) - y)Q_ZQ_Z^\top\|_2 &\leq \|\mathcal{A}^\dagger(\mathcal{A}(ZZ^\top) - y)\|_2 \\
&\leq \|\mathcal{A}^\dagger(\mathcal{A}(ZZ^\top) - y) - \mathcal{A}^\dagger(\mathcal{A}(Z_0Z_0^\top) - y) + \mathcal{A}^\dagger(\mathcal{A}(Z_0Z_0^\top) - y)\|_2 \\
&\stackrel{(i)}{\leq} (1 + \delta_{2r})\|ZZ^\top - Z_0Z_0^\top\|_F + \|\mathcal{A}^\dagger(\mathcal{A}(Z_0Z_0^\top) - y)\|_2 \\
&\leq (1 + \delta_{2r})\|ZZ^\top - U^*U^{*\top}\|_F + (1 + \delta_{2r})\|Z_0Z_0^\top - U^*U^{*\top}\|_F \\
&\quad + \|\mathcal{A}^\dagger(\mathcal{A}(Z_0Z_0^\top) - y)\|_2
\end{aligned}$$

where (i) is due to smoothness via RIP constants of the objective and the fact $\|\cdot\|_2 \leq \|\cdot\|_F$. For the first two terms on the right-hand side, we obtain:

$$\begin{aligned}
\|ZZ^\top - U^*U^{*\top}\|_F &\leq \|ZZ^\top - U^*RZ^\top + U^*RZ^\top - U^*U^{*\top}\|_F \\
&= \|(Z - U^*R)Z^\top + U^*R(Z - U^*R)^\top\|_F \\
&\leq \|Z\|_2 \cdot \|Z - U^*R\|_F + \|U^*\|_2 \cdot \|Z - U^*R\|_F \\
&\leq (\|Z\|_2 + \|U^*\|_2) \cdot \|Z - U^*R\|_F \\
&\stackrel{(i)}{\leq} \left(\sqrt{\frac{101}{99}} + \sqrt{\frac{100}{99}} \right) \|Z_0\|_2 \cdot \|Z - U^*R\|_F \\
&\stackrel{(ii)}{\leq} \left(\sqrt{\frac{101}{99}} + \sqrt{\frac{100}{99}} \right) \|Z_0\|_2 \cdot 0.00501\sigma_r(X^*)^{1/2} \\
&\leq \left(\sqrt{\frac{101}{99}} + \sqrt{\frac{100}{99}} \right) \cdot 0.00501 \cdot \sqrt{\frac{100}{99}} \cdot \|Z_0\|_2^2
\end{aligned}$$

where (i) is due to the relation of $\|Z\|_2$ and $\|U^*\|_2$ derived above, (ii) is due to Lemma 6. Similarly:

$$\|Z_0Z_0^\top - U^*U^{*\top}\|_F \leq \left(\sqrt{\frac{101}{99}} + \sqrt{\frac{100}{99}} \right) \cdot 0.00501 \cdot \sqrt{\frac{100}{99}} \cdot \|Z_0\|_2^2$$

Using these above, we obtain:

$$\|\mathcal{A}^\dagger(\mathcal{A}(ZZ^\top) - y) Q_Z Q_Z^\top\|_2 \leq \frac{2.1(1+\delta_{2r})}{100} \|Z_0Z_0^\top\|_2 + \|\mathcal{A}^\dagger(\mathcal{A}(Z_0Z_0^\top) - y)\|_2$$

Thus:

$$\begin{aligned}
\hat{\eta} &= \frac{1}{4((1+\delta_{2r})\|ZZ^\top\|_2 + \|\mathcal{A}^\dagger(\mathcal{A}(ZZ^\top) - y) Q_Z Q_Z^\top\|_2)} \\
&\geq \frac{1}{4((1+\delta_{2r})\frac{101}{99}\|Z_0Z_0\|_2 + \frac{2.1(1+\delta_{2r})}{100}\|Z_0Z_0^\top\|_2 + \|\mathcal{A}^\dagger(\mathcal{A}(Z_0Z_0^\top) - y)\|_2)} \\
&= \frac{1}{4((1+\delta_{2r})\left(\frac{101}{99} + \frac{4}{100}\right)\|Z_0Z_0^\top\|_2 + \|\mathcal{A}^\dagger(\mathcal{A}(Z_0Z_0^\top) - y)\|_2)} \\
&\geq \frac{1}{4\left(\frac{10.5}{10} \cdot (1+\delta_{2r})\|Z_0Z_0^\top\|_2 + \|\mathcal{A}^\dagger(\mathcal{A}(Z_0Z_0^\top) - y)\|_2\right)} \\
&\geq \frac{10}{10.5}\eta
\end{aligned}$$

Similarly, one gets $\hat{\eta} \leq \frac{10}{9}\eta$.

For the relation between η and η^* , we will prove here the lower bound; similar motions lead to the upper bound also. By definition, and using the relations in Corollary 3, we get:

$$\begin{aligned}
\eta &= \frac{1}{4((1+\delta_{2r})\|Z_0Z_0^\top\|_2 + \|\mathcal{A}^\dagger(\mathcal{A}(Z_0Z_0^\top) - y)\|_2)} \\
&\geq \frac{1}{4((1+\delta_{2r})\frac{101}{100}\|X^{*\top}\|_2 + \|\mathcal{A}^\dagger(\mathcal{A}(Z_0Z_0^\top) - y)\|_2)}
\end{aligned}$$

For the gradient term, we observe:

$$\begin{aligned}
\|\mathcal{A}^\dagger(\mathcal{A}(Z_0Z_0^\top) - y)\|_2 &\leq \|\mathcal{A}^\dagger(\mathcal{A}(Z_0Z_0^\top) - y) - \mathcal{A}^\dagger(\mathcal{A}(X^*) - y)\|_2 + \|\mathcal{A}^\dagger(\mathcal{A}(X^*) - y)\|_2 \\
&\stackrel{(i)}{=} \|\mathcal{A}^\dagger(\mathcal{A}(Z_0Z_0^\top) - y) - \mathcal{A}^\dagger(\mathcal{A}(X^*) - y)\|_2 \\
&\stackrel{(ii)}{\leq} (1+\delta_{2r})\|Z_0Z_0^\top - U^*U^{*\top}\|_F \\
&\stackrel{(iii)}{\leq} (1+\delta_{2r})(\|Z_0\|_2 + \|U^*\|_2) \cdot \|Z - U^*\|_F \\
&\stackrel{(iv)}{\leq} (1+\delta_{2r}) \left(\sqrt{\frac{101}{100}} + 1 \right) \|U^*\|_2 \cdot 0.00501 \cdot \|U^*\|_2^2 \\
&\leq 0.010045 \cdot (1+\delta_{2r})\|X^*\|_2
\end{aligned}$$

where (i) is due to $\|\mathcal{A}^\dagger(\mathcal{A}(X^*) - y)\|_2 = 0$, (ii) is due to the restricted smoothness assumption and the RIP, (iii) is due to the bounds above on $\|Z_0 Z_0^\top - U^* U^{*\top}\|_F$, (iv) is due to the bounds on $\|Z_0\|_2$, w.r.t. $\|U^*\|_2$, as well as the bound on $\|Z - U^* R\|_F$.

Thus, in the inequality above, we get:

$$\begin{aligned} \eta &\geq \frac{1}{4 \left((1 + \delta_{2r}) \frac{101}{100} \|X^{*\top}\|_2 + \|\mathcal{A}^\dagger(\mathcal{A}(Z_0 Z_0^\top) - y)\|_2 \right)} \\ &\geq \frac{1}{4 \left((1 + \delta_{2r}) \frac{101}{100} \|X^{*\top}\|_2 + 0.010045 \cdot (1 + \delta_{2r}) \|X^*\|_2 + \|\mathcal{A}^\dagger(\mathcal{A}(X^*) - y)\|_2 \right)} \\ &\geq \frac{1}{4 \left((1 + \delta_{2r}) \frac{102}{100} \|X^{*\top}\|_2 + \|\mathcal{A}^\dagger(\mathcal{A}(X^*) - y)\|_2 \right)} \geq \frac{100}{102} \eta^* \end{aligned}$$

Similarly, one can show that $\frac{100}{102} \eta^* \leq \eta$.

□

9 Proof of Lemma 8

The following steps follow Lemma 16 in [45]. First, denote $\Delta := Z - U^* R$.

$$\begin{aligned} &\left\langle \mathcal{A}^\dagger(\mathcal{A}(ZZ^\top) - y), (Z - U^* R)(Z - U^* R)^\top \right\rangle \\ &\stackrel{(i)}{=} \left\langle \mathcal{A}^\dagger(\mathcal{A}(ZZ^\top) - y) \cdot Q_\Delta Q_\Delta^\top, \Delta \Delta^\top \right\rangle \\ &\geq - \left| \text{Tr} \left(\mathcal{A}^\dagger(\mathcal{A}(ZZ^\top) - y) \cdot Q_\Delta Q_\Delta^\top \cdot \Delta \Delta^\top \right) \right| \\ &\stackrel{(ii)}{\geq} - \|\mathcal{A}^\dagger(\mathcal{A}(ZZ^\top) - y) \cdot Q_\Delta Q_\Delta^\top\|_2 \cdot \text{Tr}(\Delta \Delta^\top) \\ &\stackrel{(iii)}{\geq} - \left(\|\mathcal{A}^\dagger(\mathcal{A}(ZZ^\top) - y) \cdot Q_Z Q_Z^\top\|_2 + \|\mathcal{A}^\dagger(\mathcal{A}(ZZ^\top) - y) \cdot Q_{U^*} Q_{U^*}^\top\|_2 \right) \|Z - U^* R\|_F^2 \end{aligned} \quad (7)$$

Note that (i) follows from the fact $\Delta = \Delta Q_\Delta Q_\Delta^\top$, for a matrix Q that spans the row space of Δ , and (ii) follows from $|\text{Tr}(AB)| \leq \|A\|_2 \text{Tr}(B)$, for PSD matrix B (Von Neumann's trace inequality [69]). For the transformation in (iii), we use that fact that the row space of Δ , $\text{SPAN}(\Delta)$, is a subset of $\text{SPAN}(Z \cup U^*)$, as Δ is a linear combination of U and U^* .

To bound the first term in equation (7), we observe:

$$\begin{aligned} &\|\mathcal{A}^\dagger(\mathcal{A}(ZZ^\top) - y) \cdot Q_Z Q_Z^\top\|_2 \cdot \|Z - U^* R\|_F^2 \\ &\stackrel{(i)}{=} \hat{\eta} \cdot 4 \left((1 + \delta_{2r}) \|ZZ^\top\|_2 \right. \\ &\quad \left. + \|\mathcal{A}^\dagger(\mathcal{A}(ZZ^\top) - y) \cdot Q_Z Q_Z^\top\|_2 \right) \cdot \|\mathcal{A}^\dagger(\mathcal{A}(ZZ^\top) - y) \cdot Q_Z Q_Z^\top\|_2 \cdot \|Z - U^* R\|_F^2 \\ &= \underbrace{4\hat{\eta}(1 + \delta_{2r}) \|ZZ^\top\|_2 \|\mathcal{A}^\dagger(\mathcal{A}(ZZ^\top) - y) \cdot Q_Z Q_Z^\top\|_2 \cdot \|Z - U^* R\|_F^2}_{:=A} \\ &\quad + 4\hat{\eta} \|\mathcal{A}^\dagger(\mathcal{A}(ZZ^\top) - y) \cdot Q_Z Q_Z^\top\|_2^2 \cdot \|Z - U^* R\|_F^2 \end{aligned}$$

where (i) is due to the definition of $\hat{\eta}$.

To bound term A , we observe that $\|\mathcal{A}^\dagger(\mathcal{A}(ZZ^\top) - y) \cdot Q_Z Q_Z^\top\|_2 \leq \frac{(1 - \delta_{2r}) \sigma_r(ZZ^\top)}{1000}$ or $\|\mathcal{A}^\dagger(\mathcal{A}(ZZ^\top) - y) \cdot Q_Z Q_Z^\top\|_2 \geq \frac{(1 - \delta_{2r}) \sigma_r(ZZ^\top)}{1000}$. This results into bounding A as follows:

$$\begin{aligned} &4\hat{\eta}(1 + \delta_{2r}) \|ZZ^\top\|_2 \|\mathcal{A}^\dagger(\mathcal{A}(ZZ^\top) - y) \cdot Q_Z Q_Z^\top\|_2 \cdot \|Z - U^* R\|_F^2 \\ &\leq \max \left\{ \frac{4 \cdot \hat{\eta} \cdot (1 + \delta_{2r}) \|ZZ^\top\|_2 \cdot (1 - \delta_{2r}) \sigma_r(ZZ^\top)}{1000} \cdot \|Z - U^* R\|_F^2, \right. \\ &\quad \left. \hat{\eta} \cdot 4 \cdot 1000 \kappa \tau (ZZ^\top) \|\mathcal{A}^\dagger(\mathcal{A}(ZZ^\top) - y) \cdot Q_Z Q_Z^\top\|_2^2 \cdot \|Z - U^* R\|_F^2 \right\} \\ &\leq \frac{4 \cdot \hat{\eta} \cdot (1 - \delta_{2r}^2) \|ZZ^\top\|_2 \cdot \sigma_r(ZZ^\top)}{1000} \cdot \|Z - U^* R\|_F^2 \\ &\quad + \hat{\eta} \cdot 4 \cdot 1000 \kappa \tau (ZZ^\top) \|\mathcal{A}^\dagger(\mathcal{A}(ZZ^\top) - y) \cdot Q_Z Q_Z^\top\|_2^2 \cdot \|Z - U^* R\|_F^2. \end{aligned}$$

Combining the above inequalities, we obtain:

$$\begin{aligned}
& \|\mathcal{A}^\dagger(\mathcal{A}(ZZ^\top) - y) \cdot Q_Z Q_Z^\top\|_2 \cdot \|Z - U^* R\|_F^2 \\
& \stackrel{(i)}{\leq} \frac{(1-\delta_{2r})\sigma_r(ZZ^\top)}{1000} \cdot \|Z - U^* R\|_F^2 \\
& \quad + (1000\kappa\tau(ZZ^\top) + 1) \cdot 4 \cdot \hat{\eta} \|\mathcal{A}^\dagger(\mathcal{A}(ZZ^\top) - y) \cdot Q_Z Q_Z^\top\|_2^2 \cdot \|Z - U^* R\|_F^2 \\
& \stackrel{(ii)}{\leq} \frac{(1-\delta_{2r})\sigma_r(ZZ^\top)}{1000} \cdot \|Z - U^* R\|_F^2 \\
& \quad + (1000\beta^2\kappa\tau(X^*) + 1) \cdot 4 \cdot \hat{\eta} \|\mathcal{A}^\dagger(\mathcal{A}(ZZ^\top) - y) \cdot Q_Z Q_Z^\top\|_2^2 \cdot \frac{(1+2|\mu|)^2}{\kappa\tau(X^*)} \frac{1}{4 \cdot 10^4} \sigma_r(X^*) \\
& \stackrel{(iii)}{\leq} \frac{(1-\delta_{2r})\sigma_r(ZZ^\top)}{1000} \cdot \|Z - U^* R\|_F^2 \\
& \quad + 4 \cdot 1001\beta^2 \cdot \hat{\eta} \cdot \|\mathcal{A}^\dagger(\mathcal{A}(ZZ^\top) - y) \cdot Q_Z Q_Z^\top\|_2^2 \cdot \frac{(1+2|\mu|)^2}{4 \cdot 10^4 \left(1 - (1+2|\mu|)\frac{1}{200}\right)^2} \sigma_r(ZZ^\top) \\
& \stackrel{(iv)}{\leq} \frac{(1-\delta_{2r})\sigma_r(ZZ^\top)}{20} \cdot \|Z - U^* R\|_F^2 \\
& \quad + 4 \cdot 1001\beta^2 \cdot \hat{\eta} \cdot \frac{(1+2|\mu|)^2}{4 \cdot 10^4 \left(1 - (1+2|\mu|)\frac{1}{200}\right)^2} \cdot \|\mathcal{A}^\dagger(\mathcal{A}(ZZ^\top) - y) \cdot Z\|_F^2 \\
& \stackrel{(v)}{\leq} \frac{(1-\delta_{2r}) \left(1 + (1+2|\mu|)\frac{1}{200}\right)^2 \sigma_r(X^*)}{20} \cdot \|Z - U^* R\|_F^2 \\
& \quad + \frac{10.1}{100} \beta^2 \cdot \hat{\eta} \cdot \frac{(1+2|\mu|)^2}{\left(1 - (1+2|\mu|)\frac{1}{200}\right)^2} \cdot \|\mathcal{A}^\dagger(\mathcal{A}(ZZ^\top) - y) \cdot Z\|_F^2
\end{aligned}$$

where (i) follows from $\hat{\eta} \leq \frac{1}{4(1+\delta_{2r})\|ZZ^\top\|_2}$, (ii) is due to Corollary 4, bounding $\|Z - U^* R\|_F \leq \rho \sigma_r(X^*)^{1/2}$, where $\rho := (1 + 2|\mu|) \frac{1}{200\sqrt{\kappa\tau(X^*)}}$ by Lemma 6, (iii) is due to $(1000\beta^2\kappa\tau(X^*) + 1) \leq 1001\beta^2\kappa\tau(X^*)$, and by Corollary 2, (iv) is due to the fact $\sigma_r(ZZ^\top) \|\mathcal{A}^\dagger(\mathcal{A}(ZZ^\top) - y) \cdot Q_Z Q_Z^\top\|_2^2 \leq \|\mathcal{A}^\dagger(\mathcal{A}(ZZ^\top) - y) Z\|_F^2$, and (v) is due to Corollary 2.

Next, we bound the second term in equation (7):

$$\begin{aligned}
& \|\mathcal{A}^\dagger(\mathcal{A}(ZZ^\top) - y) \cdot Q_{U^*} Q_{U^*}^\top\|_2 \cdot \|Z - U^* R\|_F^2 \\
& \stackrel{(i)}{\leq} \|\mathcal{A}^\dagger(\mathcal{A}(ZZ^\top) - y) - \mathcal{A}^\dagger(\mathcal{A}(X^*) - y)\|_2 \cdot \|Z - U^* R\|_F^2 \\
& \stackrel{(ii)}{\leq} (1 + \delta_{2r}) \cdot \|ZZ^\top - U^* U^{*\top}\|_F \cdot \|Z - U^* R\|_F^2 \\
& \stackrel{(iii)}{\leq} (1 + \delta_{2r})(2 + \rho) \cdot \rho \cdot \sigma_1(U^*) \cdot \sigma_r(U^*) \cdot \|Z - U^* R\|_F^2 \\
& \stackrel{(iv)}{\leq} (1 + \delta_{2r})(2 + \rho) (1 + 2|\mu|) \cdot \frac{1}{200} \sigma_r(X^*) \cdot \|Z - U^* R\|_F^2 \\
& \leq (1 + \delta_{2r}) \left(2 + (1 + 2|\mu|) \cdot \frac{1}{200}\right) (1 + 2|\mu|) \cdot \frac{1}{200} \sigma_r(X^*) \cdot \|Z - U^* R\|_F^2,
\end{aligned}$$

where (i) follows from $\|\mathcal{A}^\dagger(\mathcal{A}(ZZ^\top) - y) \cdot Q_{U^*} Q_{U^*}^\top\|_2 \leq \|\mathcal{A}^\dagger(\mathcal{A}(ZZ^\top) - y)\|_2$ and $\mathcal{A}^\dagger(\mathcal{A}(X^*) - y) = 0$, (ii) is due to smoothness of f and the RIP constants, (iii) follows from [45, Lemma 18], for $\rho = (1 + 2|\mu|) \cdot \frac{1}{200\sqrt{\kappa\tau(X^*)}}$, (iv) follows from substituting ρ above, and observing that $\tau(X^*) = \sigma_1(U^*)^2 / \sigma_r(U^*)^2 > 1$ and $\kappa = (1 + \delta_{2r}) / (1 - \delta_{2r}) > 1$.

Combining the above we get:

$$\begin{aligned}
& \left\langle \mathcal{A}^\dagger(\mathcal{A}(ZZ^\top) - y), (Z - U^* R)(Z - U^* R)^\top \right\rangle \\
& \geq - \left(\theta \sigma_r(X^*) \cdot \|Z - U^* R\|_F^2 + \frac{10.1}{100} \beta^2 \cdot \hat{\eta} \cdot \frac{(1+2|\mu|)^2}{\left(1 - (1+2|\mu|)\frac{1}{200}\right)^2} \cdot \|\mathcal{A}^\dagger(\mathcal{A}(ZZ^\top) - y) \cdot Z\|_F^2 \right)
\end{aligned}$$

where $\theta = \frac{(1-\delta_{2r}) \left(1 + (1+2|\mu|)\frac{1}{200}\right)^2}{1000} + (1 + \delta_{2r}) \left(2 + (1 + 2|\mu|) \cdot \frac{1}{200}\right) (1 + 2|\mu|) \cdot \frac{1}{200}$.

10 Proof of Lemma 9

By smoothness assumption of the objective, based on the RIP assumption, we have:

$$\begin{aligned} \frac{1}{2}\|\mathcal{A}(ZZ^\top) - y\|_2^2 &\geq \frac{1}{2}\|\mathcal{A}(U_+U_+^\top) - y\|_2^2 \\ &\quad - \left\langle \mathcal{A}^\dagger(\mathcal{A}(ZZ^\top) - y), U_+U_+^\top - ZZ^\top \right\rangle - \frac{1+\delta_{2r}}{2}\|U_+U_+^\top - ZZ^\top\|_F^2 \Rightarrow \\ \frac{1}{2}\|\mathcal{A}(ZZ^\top) - y\|_2^2 &\geq \frac{1}{2}\|\mathcal{A}(U^*U^{*\top}) - y\|_2^2 \\ &\quad - \left\langle \mathcal{A}^\dagger(\mathcal{A}(ZZ^\top) - y), U_+U_+^\top - ZZ^\top \right\rangle - \frac{1+\delta_{2r}}{2}\|U_+U_+^\top - ZZ^\top\|_F^2 \end{aligned}$$

due to the optimality $\|\mathcal{A}(U^*U^{*\top}) - y\|_2^2 = 0 \leq \|\mathcal{A}(VV^\top) - y\|_2^2$, for any $V \in \mathbb{R}^{n \times r}$. Also, by the restricted strong convexity with RIP, we get:

$$\begin{aligned} \frac{1}{2}\|\mathcal{A}(U^*U^{*\top}) - y\|_2^2 &\geq \frac{1}{2}\|\mathcal{A}(ZZ^\top) - y\|_2^2 \\ &\quad + \left\langle \mathcal{A}^\dagger(\mathcal{A}(ZZ^\top) - y), U^*U^{*\top} - ZZ^\top \right\rangle + \frac{1-\delta_{2r}}{2}\|U^*U^{*\top} - ZZ^\top\|_F^2 \end{aligned}$$

Adding the two inequalities, we obtain:

$$\begin{aligned} \left\langle \mathcal{A}^\dagger(\mathcal{A}(ZZ^\top) - y), ZZ^\top - U^*U^{*\top} \right\rangle &\geq \left\langle \mathcal{A}^\dagger(\mathcal{A}(ZZ^\top) - y), ZZ^\top - U_+U_+^\top \right\rangle \\ &\quad - \frac{1+\delta_{2r}}{2}\|U_+U_+^\top - ZZ^\top\|_F^2 + \frac{1-\delta_{2r}}{2}\|U^*U^{*\top} - ZZ^\top\|_F^2 \end{aligned}$$

To proceed we observe:

$$\begin{aligned} U_+U_+^\top &= \left(Z - \eta\mathcal{A}^\dagger(\mathcal{A}(ZZ^\top) - y)Z \right) \cdot \left(Z - \eta\mathcal{A}^\dagger(\mathcal{A}(ZZ^\top) - y)Z \right)^\top \\ &= ZZ^\top - \eta ZZ^\top \cdot \mathcal{A}^\dagger(\mathcal{A}(ZZ^\top) - y) - \eta\mathcal{A}^\dagger(\mathcal{A}(ZZ^\top) - y) \cdot ZZ^\top \\ &\quad + \eta^2 \mathcal{A}^\dagger(\mathcal{A}(ZZ^\top) - y) \cdot ZZ^\top \cdot \mathcal{A}^\dagger(\mathcal{A}(ZZ^\top) - y) \\ &\stackrel{(i)}{=} ZZ^\top - \left(I - \frac{\eta}{2}Q_ZQ_Z^\top\mathcal{A}^\dagger(\mathcal{A}(ZZ^\top) - y) \right) \cdot \eta ZZ^\top \cdot \mathcal{A}^\dagger(\mathcal{A}(ZZ^\top) - y) \\ &\quad - \eta\mathcal{A}^\dagger(\mathcal{A}(ZZ^\top) - y) \cdot ZZ^\top \cdot \left(I - \frac{\eta}{2}Q_ZQ_Z^\top\mathcal{A}^\dagger(\mathcal{A}(ZZ^\top) - y) \right) \end{aligned}$$

where (i) is due to the fact $\mathcal{A}^\dagger(\mathcal{A}(ZZ^\top) - y) \cdot ZZ^\top \cdot \mathcal{A}^\dagger(\mathcal{A}(ZZ^\top) - y) = \mathcal{A}^\dagger(\mathcal{A}(ZZ^\top) - y) \cdot Q_ZQ_Z^\top \cdot ZZ^\top \cdot Q_ZQ_Z^\top \cdot \mathcal{A}^\dagger(\mathcal{A}(ZZ^\top) - y)$, for Q_Z a basis matrix whose columns span the column space of Z ; also, I is the identity matrix whose dimension is apparent from the context. Thus:

$$\frac{\eta}{2}Q_ZQ_Z^\top\mathcal{A}^\dagger(\mathcal{A}(ZZ^\top) - y) \leq \frac{\eta}{2}Q_ZQ_Z^\top\mathcal{A}^\dagger(\mathcal{A}(ZZ^\top) - y),$$

and, hence,

$$I - \frac{\eta}{2}Q_ZQ_Z^\top\mathcal{A}^\dagger(\mathcal{A}(ZZ^\top) - y) \succeq I - \frac{\eta}{2}Q_ZQ_Z^\top\mathcal{A}^\dagger(\mathcal{A}(ZZ^\top) - y).$$

Define $\Psi = I - \frac{\eta}{2}Q_ZQ_Z^\top\mathcal{A}^\dagger(\mathcal{A}(ZZ^\top) - y)$. Then, using the definition of $\hat{\eta}$, we know that $\hat{\eta} \leq \frac{1}{4\|Q_ZQ_Z^\top\mathcal{A}^\dagger(\mathcal{A}(ZZ^\top) - y)\|_2}$, and thus:

$$\Psi \succ 0, \quad \sigma_1(\Psi) \leq 1 + \frac{1}{4}, \quad \text{and} \quad \sigma_n(\Psi) \geq 1 - \frac{1}{4}.$$

Going back to the main recursion and using the above expression for $U_+U_+^\top$, we have:

$$\begin{aligned}
& \left\langle \mathcal{A}^\dagger(\mathcal{A}(ZZ^\top) - y), ZZ^\top - U^*U^{*\top} \right\rangle - \frac{1-\delta_{2r}}{2} \|U^*U^{*\top} - ZZ^\top\|_F^2 \\
& \geq \left\langle \mathcal{A}^\dagger(\mathcal{A}(ZZ^\top) - y), ZZ^\top - U_+U_+^\top \right\rangle - \frac{1+\delta_{2r}}{2} \|U_+U_+^\top - ZZ^\top\|_F^2 \\
& \stackrel{(i)}{\geq} 2\eta \left\langle \mathcal{A}^\dagger(\mathcal{A}(ZZ^\top) - y), \mathcal{A}^\dagger(\mathcal{A}(ZZ^\top) - y) \cdot ZZ^\top \cdot \Psi \right\rangle \\
& \quad - \frac{1+\delta_{2r}}{2} \|2\eta \mathcal{A}^\dagger(\mathcal{A}(ZZ^\top) - y) \cdot ZZ^\top \cdot \Psi\|_F^2 \\
& \stackrel{(ii)}{\geq} \frac{7}{4}\eta \left\| \mathcal{A}^\dagger(\mathcal{A}(ZZ^\top) - y) Z \right\|_F^2 \\
& \quad - 2(1 + \delta_{2r})\eta^2 \left\| \mathcal{A}^\dagger(\mathcal{A}(ZZ^\top) - y) Z \right\|_F^2 \cdot \|Z\|_2^2 \cdot \|\Psi\|_2^2 \\
& \stackrel{(iii)}{\geq} \frac{7}{4}\eta \left\| \mathcal{A}^\dagger(\mathcal{A}(ZZ^\top) - y) Z \right\|_F^2 \\
& \quad - 2(1 + \delta_{2r})\eta^2 \left\| \mathcal{A}^\dagger(\mathcal{A}(ZZ^\top) - y) Z \right\|_F^2 \cdot \|Z\|_2^2 \cdot \left(\frac{9}{8}\right)^2 \\
& = \frac{7}{4}\eta \left\| \mathcal{A}^\dagger(\mathcal{A}(ZZ^\top) - y) Z \right\|_F^2 \cdot \left(1 - 2(1 + \delta_{2r})\eta \cdot \|Z\|_2^2 \cdot \left(\frac{9}{8}\right)^2 \cdot \frac{4}{7}\right) \\
& \stackrel{(iv)}{\geq} \frac{7}{4}\eta \left\| \mathcal{A}^\dagger(\mathcal{A}(ZZ^\top) - y) Z \right\|_F^2 \cdot \left(1 - 2(1 + \delta_{2r})\hat{\eta} \cdot \|Z\|_2^2 \cdot \left(\frac{9}{8}\right)^2 \cdot \frac{4}{7}\right) \\
& \stackrel{(v)}{\geq} \frac{7}{4}\eta \left\| \mathcal{A}^\dagger(\mathcal{A}(ZZ^\top) - y) Z \right\|_F^2 \cdot \left(1 - \frac{2 \cdot \left(\frac{9}{8}\right)^2}{7}\right) \\
& = 1.1172\eta \left\| \mathcal{A}^\dagger(\mathcal{A}(ZZ^\top) - y) Z \right\|_F^2
\end{aligned}$$

where (i) is due to the symmetry of the objective; (ii) is due to Cauchy-Schwartz inequality and the fact:

$$\begin{aligned}
& \left\langle \mathcal{A}^\dagger(\mathcal{A}(ZZ^\top) - y), \mathcal{A}^\dagger(\mathcal{A}(ZZ^\top) - y) \cdot ZZ^\top \cdot \Psi \right\rangle \\
& = \left\langle \mathcal{A}^\dagger(\mathcal{A}(ZZ^\top) - y), \mathcal{A}^\dagger(\mathcal{A}(ZZ^\top) - y) \cdot ZZ^\top \right\rangle \\
& \quad - \frac{\eta}{2} \left\langle \mathcal{A}^\dagger(\mathcal{A}(ZZ^\top) - y), \mathcal{A}^\dagger(\mathcal{A}(ZZ^\top) - y) \cdot ZZ^\top \cdot \mathcal{A}^\dagger(\mathcal{A}(ZZ^\top) - y) \right\rangle \\
& \stackrel{(i)}{\geq} \left\langle \mathcal{A}^\dagger(\mathcal{A}(ZZ^\top) - y), \mathcal{A}^\dagger(\mathcal{A}(ZZ^\top) - y) \cdot ZZ^\top \right\rangle \\
& \quad - \frac{\hat{\eta}}{2} \left\langle \mathcal{A}^\dagger(\mathcal{A}(ZZ^\top) - y), \mathcal{A}^\dagger(\mathcal{A}(ZZ^\top) - y) \cdot ZZ^\top \cdot \mathcal{A}^\dagger(\mathcal{A}(ZZ^\top) - y) \right\rangle \\
& \geq \left(1 - \frac{\hat{\eta}}{2} \|Q_Z Q_Z^\top \mathcal{A}^\dagger(\mathcal{A}(ZZ^\top) - y)\|_2^2\right) \cdot \left\| \mathcal{A}^\dagger(\mathcal{A}(ZZ^\top) - y) Z \right\|_F^2 \\
& \geq \left(1 - \frac{1}{4}\right) \left\| \mathcal{A}^\dagger(\mathcal{A}(ZZ^\top) - y) Z \right\|_F^2
\end{aligned}$$

where (i) is due to $\eta \leq \hat{\eta}$, and the last inequality comes from the definition of the $\hat{\eta}$ and its upper bound; (iii) is due to the upper bound on $\|\Psi\|_2$ above; (iv) is due to $\eta \leq \hat{\eta}$; (v) is due to $\hat{\eta} \leq \frac{1}{4(1+\delta_{2r})\|ZZ^\top\|_2}$.

The above lead to the desiderata:

$$\left\langle \mathcal{A}^\dagger(\mathcal{A}(ZZ^\top) - y), ZZ^\top - U^*U^{*\top} \right\rangle \geq 1.1172\eta \left\| \mathcal{A}^\dagger(\mathcal{A}(ZZ^\top) - y) Z \right\|_F^2 + \frac{1-\delta_{2r}}{2} \|U^*U^{*\top} - ZZ^\top\|_F^2$$

11 Full proof of Theorem 1

We first denote $U_+ \equiv U_{i+1}$, $U \equiv U_i$, $U_- \equiv U_{i-1}$ and $Z \equiv Z_i$. Let us start with the following equality. Given that U_0 is close enough the solution U^*R , for some $R \in \mathcal{O}$,⁸ we have:

$$\begin{aligned}
\|U_+ - U^*R\|_F^2 &= \|U_+ - Z + Z - U^*R\|_F^2 \\
&= \|U_+ - Z\|_F^2 + \|Z - U^*R\|_F^2 - 2\langle U_+ - Z, U^*R - Z \rangle
\end{aligned}$$

⁸We assume that the initialization condition places the algorithm to a initial point where R remains the same during the execution; *i.e.*, the algorithm moves towards a minimum for a fixed R .

The proof focuses on how to bound the last part on the right-hand side. By definition of U_+ , we get:

$$\begin{aligned}\langle U_+ - Z, U^*R - Z \rangle &= \langle Z - \eta \mathcal{A}^\dagger(\mathcal{A}(ZZ^\top) - y) Z - Z, U^*R - Z \rangle \\ &= \eta \langle \mathcal{A}^\dagger(\mathcal{A}(ZZ^\top) - y) Z, Z - U^*R \rangle\end{aligned}$$

Observe the following:

$$\begin{aligned}\langle \mathcal{A}^\dagger(\mathcal{A}(ZZ^\top) - y) Z, Z - U^*R \rangle &= \langle \mathcal{A}^\dagger(\mathcal{A}(ZZ^\top) - y), ZZ^\top - U^*RZ^\top \rangle \\ &= \langle \mathcal{A}^\dagger(\mathcal{A}(ZZ^\top) - y), ZZ^\top - \frac{1}{2}U^*U^{*\top} + \frac{1}{2}U^*U^{*\top} - U^*RZ^\top \rangle \\ &= \frac{1}{2} \langle \mathcal{A}^\dagger(\mathcal{A}(ZZ^\top) - y), ZZ^\top - U^*U^{*\top} \rangle \\ &\quad + \langle \mathcal{A}^\dagger(\mathcal{A}(ZZ^\top) - y), \frac{1}{2}(ZZ^\top + U^*U^{*\top}) - U^*RZ^\top \rangle \\ &= \frac{1}{2} \langle \mathcal{A}^\dagger(\mathcal{A}(ZZ^\top) - y), ZZ^\top - U^*U^{*\top} \rangle \\ &\quad + \frac{1}{2} \langle \mathcal{A}^\dagger(\mathcal{A}(ZZ^\top) - y), (Z - U^*R)(Z - U^*R)^\top \rangle\end{aligned}$$

To proceed, we will use the following two lemmata; their proof is provided in the appendices 9 and 10, respectively.

Lemma 8. *Let $U \in \mathbb{R}^{n \times r}$, $U_- \in \mathbb{R}^{n \times r}$, and $U^* \in \mathbb{R}^{n \times r}$, such that $\|U - U^*R\|_F \leq \frac{\sigma_r(X^*)^{1/2}}{200\sqrt{\kappa\tau(X^*)}}$ and $\|U_- - U^*R\|_F \leq \frac{\sigma_r(X^*)^{1/2}}{200\sqrt{\kappa\tau(X^*)}}$, where $X^* = U^*U^{*\top}$, and $\kappa := \frac{1+\delta_{2r}}{1-\delta_{2r}} > 1$, for $\delta_{2r} \leq \frac{1}{10}$, and $\tau(X^*) := \frac{\sigma_1(X^*)}{\sigma_r(X^*)} > 1$. By Lemma 6, the above imply also that: $\|Z - U^*R\|_F \leq (1 + 2|\mu|) \cdot \frac{\sigma_r(X^*)^{1/2}}{200}$. Then, under RIP assumptions of the mapping \mathcal{A} , we have:*

$$\begin{aligned}&\langle \mathcal{A}^\dagger(\mathcal{A}(ZZ^\top) - y), (Z - U^*R)(Z - U^*R)^\top \rangle \\ &\geq - \left(\theta \sigma_r(X^*) \cdot \|Z - U^*R\|_F^2 + \frac{10.1}{100} \beta^2 \cdot \hat{\eta} \cdot \frac{(1+2|\mu|)^2}{\left(1 - \frac{1}{200}(1+2|\mu|)\right)^2} \cdot \|\mathcal{A}^\dagger(\mathcal{A}(ZZ^\top) - y) \cdot Z\|_F^2 \right)\end{aligned}$$

$$\text{where } \theta = \frac{(1-\delta_{2r})\left(1 + \frac{1}{200}(1+2|\mu|)\right)^2}{1000} + (1 + \delta_{2r}) \left(2 + \frac{1}{200}(1+2|\mu|)\right) (1 + 2|\mu|) \cdot \frac{1}{200}, \quad \text{and } \hat{\eta} = \frac{1}{4((1+\delta_r)\|ZZ^\top\|_2 + \|\mathcal{A}^\dagger(\mathcal{A}(ZZ^\top) - y)Q_Z Q_Z^\top\|_2)}.$$

From Lemma 8, we derive the following corollary.

Corollary 5. *Under the assumptions of Lemma 8, and assuming $\delta_{2r} \leq \frac{1}{10}$ and $\mu = \frac{1}{1000}$, Lemma 8 transforms into:*

$$\begin{aligned}&\langle \mathcal{A}^\dagger(\mathcal{A}(ZZ^\top) - y), (Z - U^*R)(Z - U^*R)^\top \rangle \\ &\geq - \left(\frac{1.4}{100} \cdot (1 - \delta_{2r}) \cdot \sigma_r(X^*) \cdot \|Z - U^*R\|_F^2 + 0.1049 \cdot \|\mathcal{A}^\dagger(\mathcal{A}(ZZ^\top) - y) \cdot Z\|_F^2 \right)\end{aligned}$$

Lemma 9. *Under similar assumptions with Lemma 8, the following inequality holds:*

$$\langle \mathcal{A}^\dagger(\mathcal{A}(ZZ^\top) - y), ZZ^\top - U^*U^{*\top} \rangle \geq 1.1172\eta \left\| \mathcal{A}^\dagger(\mathcal{A}(ZZ^\top) - y) Z \right\|_F^2 + \frac{1-\delta_{2r}}{2} \|U^*U^{*\top} - ZZ^\top\|_F^2$$

Going back to our original equation, we have:

$$\begin{aligned}\|U_+ - U^*R\|_F^2 &= \|U_+ - Z\|_F^2 + \|Z - U^*R\|_F^2 - 2\langle U_+ - Z, U^*R - Z \rangle \\ &= \eta^2 \|\mathcal{A}^\dagger(\mathcal{A}(ZZ^\top) - y) Z\|_F^2 + \|Z - U^*R\|_F^2 \\ &\quad - \eta \langle \mathcal{A}^\dagger(\mathcal{A}(ZZ^\top) - y), ZZ^\top - U^*U^{*\top} \rangle \\ &\quad - \eta \langle \mathcal{A}^\dagger(\mathcal{A}(ZZ^\top) - y), (Z - U^*R)(Z - U^*R)^\top \rangle \\ &\leq \|U_+ - Z\|_F^2 + \|Z - U^*R\|_F^2 \\ &\quad - 1.1172\eta^2 \left\| \mathcal{A}^\dagger(\mathcal{A}(ZZ^\top) - y) Z \right\|_F^2 - \eta \frac{1-\delta_{2r}}{2} \|U^*U^{*\top} - ZZ^\top\|_F^2 \\ &\quad + \eta \left(\theta \sigma_r(X^*) \cdot \|Z - U^*R\|_F^2 \right. \\ &\quad \left. + \frac{10.1}{100} \beta^2 \cdot \hat{\eta} \cdot \frac{(1+2|\mu|)^2}{\left(1 - \frac{1}{200}(1+2|\mu|)\right)^2} \cdot \|\mathcal{A}^\dagger(\mathcal{A}(ZZ^\top) - y) \cdot Z\|_F^2 \right)\end{aligned}$$

Next, we use the following lemma:

Lemma 10. [34, Lemma 5.4] For any $W, V \in \mathbb{R}^{n \times r}$, the following holds:

$$\|WW^\top - VV^\top\|_F^2 \geq 2(\sqrt{2} - 1) \cdot \sigma_r(VV^\top) \cdot \text{DIST}(W, V)^2.$$

Thus, the quantity $\|U^*U^{*\top} - ZZ^\top\|_F^2$ above satisfies:

$$\|U^*U^{*\top} - ZZ^\top\|_F^2 \geq 2(\sqrt{2} - 1) \cdot \sigma_r(X^*) \cdot \|Z - U^*R\|_F^2,$$

which, in our main recursion, results in:

$$\begin{aligned} \|U_+ - U^*R\|_F^2 &\leq \|U_+ - Z\|_F^2 + \|Z - U^*R\|_F^2 \\ &\quad - 1.1172\eta^2 \left\| \mathcal{A}^\dagger(\mathcal{A}(ZZ^\top) - y)Z \right\|_F^2 - \eta(\sqrt{2} - 1)(1 - \delta_{2r})\sigma_r(X^*)\|Z - U^*R\|_F^2 \\ &\quad + \eta \left(\theta\sigma_r(X^*) \cdot \|Z - U^*R\|_F^2 \right. \\ &\quad \left. + \frac{10.1}{100}\beta^2 \cdot \hat{\eta} \cdot \frac{(1+2|\mu|)^2}{\left(1 - \frac{1}{200}(1+2|\mu|)\right)^2} \cdot \|\mathcal{A}^\dagger(\mathcal{A}(ZZ^\top) - y) \cdot Z\|_F^2 \right) \\ &\stackrel{(i)}{\leq} \|U_+ - Z\|_F^2 + \|Z - U^*R\|_F^2 \\ &\quad - 1.1172\eta^2 \left\| \mathcal{A}^\dagger(\mathcal{A}(ZZ^\top) - y)Z \right\|_F^2 - \eta(\sqrt{2} - 1)(1 - \delta_{2r})\sigma_r(X^*)\|Z - U^*R\|_F^2 \\ &\quad + \eta \left(\theta\sigma_r(X^*) \cdot \|Z - U^*R\|_F^2 \right. \\ &\quad \left. + \frac{10.1}{100}\beta^2 \cdot \frac{10}{9}\eta \cdot \frac{(1+2|\mu|)^2}{\left(1 - \frac{1}{200}(1+2|\mu|)\right)^2} \cdot \|\mathcal{A}^\dagger(\mathcal{A}(ZZ^\top) - y) \cdot Z\|_F^2 \right) \\ &\stackrel{(ii)}{=} \left(1 + \frac{10.1}{100}\beta^2 \cdot \frac{10}{9} \cdot \frac{(1+2|\mu|)^2}{\left(1 - \frac{1}{200}(1+2|\mu|)\right)^2} - 1.1172 \right) \eta^2 \|\mathcal{A}^\dagger(\mathcal{A}(ZZ^\top) - y) \cdot Z\|_F^2 \\ &\quad + \left(1 + \theta\sigma_r(X^*) - \eta(\sqrt{2} - 1)(1 - \delta_{2r})\sigma_r(X^*) \right) \|Z - U^*R\|_F^2 \end{aligned}$$

where (i) is due to Lemma 7, and (ii) is due to the definition of U_+ .

Remark 4. The discussion so far holds without any assumption on μ ; in the discussion below, we will set $\mu = \frac{1}{1000}$; in practice, larger values for μ still lead to accelerated convergence in our experiments, which implies that the proof can be improved for stricter initialization assumptions and different μ values. Different μ values lead to different conditions for the main quantities/assumptions involved.

Assuming $\mu = \frac{1}{1000}$ and $\delta_{2r} \leq \frac{1}{10}$, the main constant quantities in our proof so far simplify into:

$$\beta = \frac{1 + (1 + 2|\mu|) \cdot \frac{1}{200}}{1 - (1 + 2|\mu|) \cdot \frac{1}{200}} = 1.0121, \quad \text{and} \quad \beta^2 = 1.0202,$$

and thus,

$$\frac{10.1}{100}\beta^2 \cdot \frac{10}{9} \cdot \frac{(1+2|\mu|)^2}{\left(1 - \frac{1}{200}(1+2|\mu|)\right)^2} = 0.1166,$$

and, finally,

$$\begin{aligned} \theta &= \frac{(1 - \delta_{2r}) \left(1 + \frac{1}{200}(1 + 2|\mu|)\right)^2}{1000} + (1 + \delta_{2r}) \left(2 + (1 + 2|\mu|) \cdot \frac{1}{200}\right) (1 + 2|\mu|) \cdot \frac{1}{200} \\ &\stackrel{(i)}{=} (1 - \delta_{2r}) \cdot \left(\frac{\left(1 + \frac{1}{200}(1 + 2|\mu|)\right)^2}{1000} + \kappa \left(2 + (1 + 2|\mu|) \cdot \frac{1}{200}\right) (1 + 2|\mu|) \cdot \frac{1}{200} \right) \\ &\leq (1 - \delta_{2r}) \cdot 0.0134. \end{aligned}$$

where (i) is by definition of $\kappa := \frac{1+\delta_{2r}}{1-\delta_{2r}} \leq 1.223$ for $\delta_{2r} \leq \frac{1}{10}$, by assumption. Combining the above in our main inequality, we obtain:

$$\begin{aligned}
\|U_+ - U^*R\|_F^2 &\leq (1 + 0.1166 - 1.1172) \eta^2 \|\mathcal{A}^\dagger(\mathcal{A}(ZZ^\top) - y) \cdot Z\|_F^2 \\
&\quad + \left(1 + 0.0134 \cdot \eta(1 - \delta_{2r})\sigma_r(X^*) - \eta(\sqrt{2} - 1)(1 - \delta_{2r})\sigma_r(X^*)\right) \|Z - U^*R\|_F^2 \\
&= -6 \cdot 10^{-4} \eta^2 \|\mathcal{A}^\dagger(\mathcal{A}(ZZ^\top) - y) \cdot Z\|_F^2 \\
&\quad + \left(1 + \eta\sigma_r(X^*)(1 - \delta_{2r}) \cdot (0.0134 - \sqrt{2} + 1)\right) \|Z - U^*R\|_F^2 \\
&\leq \left(1 + \eta\sigma_r(X^*)(1 - \delta_{2r}) \cdot (0.0134 - \sqrt{2} + 1)\right) \|Z - U^*R\|_F^2 \\
&\leq \left(1 - \frac{4\eta\sigma_r(X^*)(1-\delta_{2r})}{10}\right) \|Z - U^*R\|_F^2
\end{aligned} \tag{8}$$

By Lemma 7, we know that $\eta \geq \frac{100}{102}\eta^*$. Also, $\eta^* = \frac{1}{4(1+\delta_{2r})\|X^*\|_2}$, since $\|\mathcal{A}^\dagger(\mathcal{A}(X^*) - y)\|_2 = 0$, in the noiseless setting. Returning to (8), we have:

$$\begin{aligned}
\|U_+ - U^*R\|_F^2 &\leq \left(1 - 0.393 \cdot \frac{(1-\delta_{2r})\sigma_r(X^*)}{(1+\delta_{2r})\sigma_1(X^*)}\right) \|Z - U^*R\|_F^2 \\
&= \left(1 - \frac{0.393}{\kappa\tau(X^*)}\right) \|Z - U^*R\|_F^2
\end{aligned}$$

Taking square root on both sides, we obtain:

$$\|U_+ - U^*R\|_F \leq \sqrt{1 - \frac{0.393}{\kappa\tau(X^*)}} \|Z - U^*R\|_F$$

We know that, for $|x| \leq 1$, the following bounds hold:

$$\sqrt{1+x} \leq e^{x/2} \leq \sqrt{1+x+x^2}.$$

Setting $x = -\frac{0.393}{\kappa\tau(X^*)}$, we have:

$$\|U_+ - U^*R\|_F \leq e^{-\frac{0.393}{2\kappa\tau(X^*)}} \|Z - U^*R\|_F \leq e^{-\frac{4}{25\tau(X^*)}} \|Z - U^*R\|_F,$$

where $\kappa = \frac{1+\delta_{2r}}{1-\delta_{2r}} \leq \frac{11}{9}$, assuming $\delta_{2r} \leq \frac{1}{10}$.

Using the definition of Z , $Z = U + \tau(U - U_-)$, we get

$$\begin{aligned}
\|U_+ - U^*R\|_F &\leq e^{-\frac{4}{25\tau(X^*)}} \|U + \tau(U - U_-) - U^*R\|_F \\
&= e^{-\frac{4}{25\tau(X^*)}} \|U + \tau(U - U_-) - (1 - \tau + \tau)U^*R\|_F \\
&= e^{-\frac{4}{25\tau(X^*)}} \|(1 + \tau)(U - U^*R) + \tau(U^*R - U_-)\|_F \\
&= e^{-\frac{4}{25\tau(X^*)}} \|(1 + \tau)(U - U^*R) + \tau(U^*R - U_-)\|_F \\
&\leq e^{-\frac{4}{25\tau(X^*)}} \cdot |1 + \mu| \cdot \|U - U^*R\|_F + e^{-\frac{4}{25\tau(X^*)}} \cdot |\mu| \cdot \|U_- - U^*R\|_F
\end{aligned}$$

Define $h(i) = \|U_i - U^*R\|_F$; this leads to the following second-order linear system:

$$h(i+1) \leq e^{-\frac{4}{25\tau(X^*)}} \cdot |1 + \mu| \cdot h(i) + e^{-\frac{4}{25\tau(X^*)}} \cdot |\mu| \cdot h(i-1).$$

We can convert this second-order linear system into a two-dimensional first-order system, where the variables of the linear system are multi-dimensional. To do this, we define a new state variable $q(i)$:

$$q(i) := h(i+1).$$

Using $q(i)$, we define the following 2-dimensional, first-order system:

$$\begin{cases} q(i) - e^{-\frac{4}{25\tau(X^*)}} \cdot |1 + \mu| \cdot h(i) - e^{-\frac{4}{25\tau(X^*)}} \cdot |\mu| \cdot h(i-1) \leq 0, \\ h(i) \leq q(i-1). \end{cases}$$

This further characterizes the evolution of two state variables, $\{q(i), h(i)\}$:

$$\begin{aligned}
\begin{bmatrix} q(i) \\ h(i) \end{bmatrix} &\leq \begin{bmatrix} e^{-\frac{4}{25\tau(X^*)}} \cdot |1 + \mu| & e^{-\frac{4}{25\tau(X^*)}} \cdot |\mu| \\ 1 & 0 \end{bmatrix} \cdot \begin{bmatrix} q(i-1) \\ h(i-1) \end{bmatrix} \Rightarrow \\
\begin{bmatrix} \|U_{i+1} - U^*R\|_F \\ \|U_i - U^*R\|_F \end{bmatrix} &\leq \begin{bmatrix} e^{-\frac{4}{25\tau(X^*)}} \cdot |1 + \mu| & e^{-\frac{4}{25\tau(X^*)}} \cdot |\mu| \\ 1 & 0 \end{bmatrix} \cdot \begin{bmatrix} \|U_i - U^*R\|_F \\ \|U_{i-1} - U^*R\|_F \end{bmatrix},
\end{aligned}$$

where in the last inequality we use the definitions $h(i) = \|U_i - U^*R\|_F$ and $q(i) = h(i+1)$. Observe that the contraction matrix has non-negative values.

Define $A := \begin{bmatrix} e^{-\frac{4}{25\tau(X^*)}} \cdot |1 + \mu| & e^{-\frac{4}{25\tau(X^*)}} \cdot |\mu| \\ 1 & 0 \end{bmatrix}$. Unfolding the above recursion for J iterations, we obtain:

$$\begin{bmatrix} \|U_{J+1} - U^*R\|_F \\ \|U_J - U^*R\|_F \end{bmatrix} \leq A^J \cdot \begin{bmatrix} \|U_1 - U^*R\|_F \\ \|U_0 - U^*R\|_F \end{bmatrix}.$$

Define $y(i) = \begin{bmatrix} \|U_{i+1} - U^*R\|_F \\ \|U_i - U^*R\|_F \end{bmatrix}$; then, the above expression becomes

$$y(T) \leq A^{J+1} \cdot y(-1).$$

A has only non-negative values. Here, we make the convention that $\|U_{-1} - U^*R\|_F = \|U_0 - U^*R\|_F$, such that $y(-1) = \begin{bmatrix} 1 \\ 1 \end{bmatrix} \cdot \|U_0 - U^*R\|_F$.

Let us focus on the properties of the matrix A . We re-use Lemma 2 in [22], after appropriate changes:

Lemma 11. *Let A be the 2×2 matrix, as defined above, parameterized by $\xi := e^{-\frac{4}{25\tau(X^*)}} > 0$, and user-defined parameter μ . The characteristic polynomial of A is defined as:*

$$\lambda^2 - \text{Tr}(A) \cdot \lambda + \det(A) = 0$$

where λ represent the eigenvalue(s) of A . Define $\Delta := \text{Tr}(A)^2 - 4 \cdot \det(A) = \xi^2 \cdot (1 + \mu)^2 + 4\xi \cdot |\mu|$. Then, the eigenvalues of A satisfy the expression: $\lambda_{1,2} = \frac{\xi \cdot |1 + \mu| \pm \sqrt{\Delta}}{2}$.

In our case, $\Delta > 0$, which means that $\lambda_{1,2} = \frac{e^{-\frac{4}{25\tau(X^*)}} \cdot |1 + \mu| \pm \sqrt{e^{-\frac{8}{25\tau(X^*)}} (1 + \mu)^2 + 4e^{-\frac{4}{25\tau(X^*)}} |\mu|}}{2}$. The following lemma describes how one can compute a power of a 2×2 matrix A , A^i , through the eigenvalues $\lambda_{1,2}$ (real and distinct eigenvalues); the proof is provided in [22].

Lemma 12 ([55]). *Let A be a 2×2 matrix with real eigenvalues $\lambda_{1,2}$. Then, the following expression holds, when $\lambda_1 \neq \lambda_2$:*

$$A^i = \frac{\lambda_1^i - \lambda_2^i}{\lambda_1 - \lambda_2} \cdot A - \lambda_1 \lambda_2 \cdot \frac{\lambda_1^{i-1} - \lambda_2^{i-1}}{\lambda_1 - \lambda_2} \cdot I$$

where λ_i denotes the i -th eigenvalue of A in order.

Then, the main recursion takes the following form:

$$y(J) \leq \frac{\lambda_1^{J+1} - \lambda_2^{J+1}}{\lambda_1 - \lambda_2} \cdot A \cdot y(-1) - \lambda_1 \lambda_2 \frac{\lambda_1^J - \lambda_2^J}{\lambda_1 - \lambda_2} \cdot y(-1).$$

Observe that, in order to achieve convergence (i.e., the RHS converges to zero), eigenvalues of A play a crucial role: Both A and $y(-1)$ are constant quantities, and only how fast the quantities $\lambda_1^{J+1} - \lambda_2^{J+1}$ and $\lambda_1^J - \lambda_2^J$ “shrink” matter most. The above suggest that we require $|\lambda_{1,2}| < 1$ for convergence. To achieve this, we require:

$$|\lambda_{1,2}| \leq \left| \frac{1}{2} e^{-\frac{4}{25\tau(X^*)}} \cdot |1 + \mu| \right| + \left| \frac{1}{2} \sqrt{e^{-\frac{8}{25\tau(X^*)}} (1 + \mu)^2 + 4e^{-\frac{4}{25\tau(X^*)}} \cdot |\mu|} \right| \leq 1$$

under the assumption that $\mu = \frac{1}{1000}$, the above expression becomes:

$$|\lambda_{1,2}| \leq 0.853e^{\frac{1}{\tau(X^*)}} + 0.855e^{\frac{1}{2\tau(X^*)}} - 2 \leq 0.$$

This is satisfied for any X^* such that:

$$\tau(X^*) \leq 3.3209,$$

which is the assumption made in the theorem.

Using the assumption $|\lambda_{1,2}| < 1$, our main recursion further transforms to:

$$\begin{aligned} y(J) &\leq \frac{\lambda_1^{J+1} - \lambda_2^{J+1}}{\lambda_1 - \lambda_2} \cdot A \cdot y(-1) - \lambda_1 \lambda_2 \frac{\lambda_1^J - \lambda_2^J}{\lambda_1 - \lambda_2} \cdot y(-1) \\ &\stackrel{(i)}{\leq} \frac{|\lambda_1|^{J+1} + |\lambda_2|^{J+1}}{|\lambda_1| - |\lambda_2|} \cdot A \cdot y(-1) + |\lambda_1 \lambda_2| \cdot \frac{|\lambda_1|^J + |\lambda_2|^J}{|\lambda_1| - |\lambda_2|} \cdot y(-1) \\ &\stackrel{(ii)}{\leq} \frac{2|\lambda_1|^{J+1}}{|\lambda_1| - |\lambda_2|} \cdot A \cdot y(-1) + |\lambda_1| \cdot \frac{2|\lambda_1|^J}{|\lambda_1| - |\lambda_2|} \cdot y(-1) \end{aligned}$$

where (i) is due to $A \cdot y(-1)$ and $y(-1)$ being positive quantities, and (ii) is due to $1 > |\lambda_1| > |\lambda_2|$.

Focusing on the first entry of $y(J)$, we get:

$$\begin{aligned} \|U_{J+1} - U^* R\|_F &\leq \frac{2|\lambda_1|^{J+1}}{|\lambda_1| - |\lambda_2|} \cdot e^{-\frac{4}{25\tau(X^*)}} \cdot (1 + \mu + |\mu|) \cdot \|U_0 - U^* R\|_F + \frac{2|\lambda_1|^{J+1}}{|\lambda_1| - |\lambda_2|} \cdot \|U_0 - U^* R\|_F \\ &\leq \frac{2|\lambda_1|^{J+1}}{|\lambda_1| - |\lambda_2|} \cdot \left(e^{-\frac{4}{25\tau(X^*)}} \cdot (1 + \mu + |\mu|) + 1 \right) \cdot \|U_0 - U^* R\|_F \end{aligned}$$

This suggests that, as long as $|\lambda_{1,2}| < 1$, the first term on the right-hand side “shrinks” exponentially with rate $|\lambda_1|^{J+1}$, but also depends (inverse proportionally) on the spectral gap $|\lambda_1| - |\lambda_2|$. In the noiseless case where $\varepsilon = 0$, the above result guarantees convergence.

12 Synthetic experiments

In this set of experiments, we compare Accelerated Procrustes Flow with **(i)** the Matrix ALPS framework [21], a projected gradient descent algorithm, operating on the full matrix variable X , with adaptive step size η —this algorithm has outperformed most of the schemes that work on the original space X ; **(ii)** the plain Procrustes Flow algorithm [34], where we use the step size as reported in [45], since the later has reported better performance than vanilla Procrustes Flow. Further, the original Procrustes Flow algorithm relies on performing many iterations in the original space X as an initialization scheme, which is often prohibitive as the problem dimensions grow. Both for our algorithm and the plain Procrustes Flow scheme, we use both random and specific initializations, according to Lemma 1.

Implementation details. To properly compare the algorithms in the above list, we preset a set of parameters that are common. We fix the dimension $n = 4096$ and the rank of the optimal matrix $X^* \in \mathbb{R}^{n \times n}$ to be $r = 50$. We fix the number of observables m to be $m = C \cdot n \times r$, where $C \in \{3, 5\}$. All algorithms in comparison are implemented in MATLAB. In all algorithms, we fix the maximum number of iterations to 4000, and we use the same stopping criterion: $\frac{\|X_{i+1} - X_i\|_F}{\|X_i\|_F} \leq \text{tol}$, where $\text{tol} := 5 \cdot 10^{-5}$.

For the implementation of the Accelerated Procrustes Flow, we have used $\mu = \frac{2}{3}$. This value is larger than what our theory dictates, but as we have conjectured, our theory holds for different configurations of (μ, δ_{2r}) ; proving our theory for a less strict feasible values of these parameters remains an open problem. Moreover, we have observed that various values of μ still lead to acceleration; in our experiments, we selected μ using grid search over the set $\{\frac{1}{4}, \frac{1}{2}, \frac{2}{3}, \frac{3}{4}\}$.

Problem setup. The set of experiments are set to:

$$y = \mathcal{A}(X^*) + w;$$

while the theory holds for the noiseless case, we show empirically that noisy cases are nicely handled by the same algorithm. We use permuted and subsampled noiselets for the linear operator \mathcal{A} [39]. The optimal matrix X^* is generated as the multiplication of a tall matrix $U^* \in \mathbb{R}^{n \times r}$ such that $X^* = U^* U^{*\top}$, and $\|X^*\|_F = 1$, without loss of generality. The entries of U^* are drawn i.i.d. from a Gaussian distribution with zero mean and unit variance. In the single noisy case, w has the same dimensions with y , its entries are drawn from a zero mean Gaussian distribution with norm $\|w\|_2 = 0.01$.

The results are shown in Figure 5. In all cases, our findings illustrate the effectiveness of the proposed schemes on different problem configurations.

13 μ ECoG simulation details

In section 6, we presented a novel Neuroscience application for low rank matrix sensing and our accelerated Procrustes flow algorithm. We presented results for recovering individual neuron activities from stimulus evoked cortical surface electrical potentials (μ ECoG). Here, we give additional details and results related to this experiment.

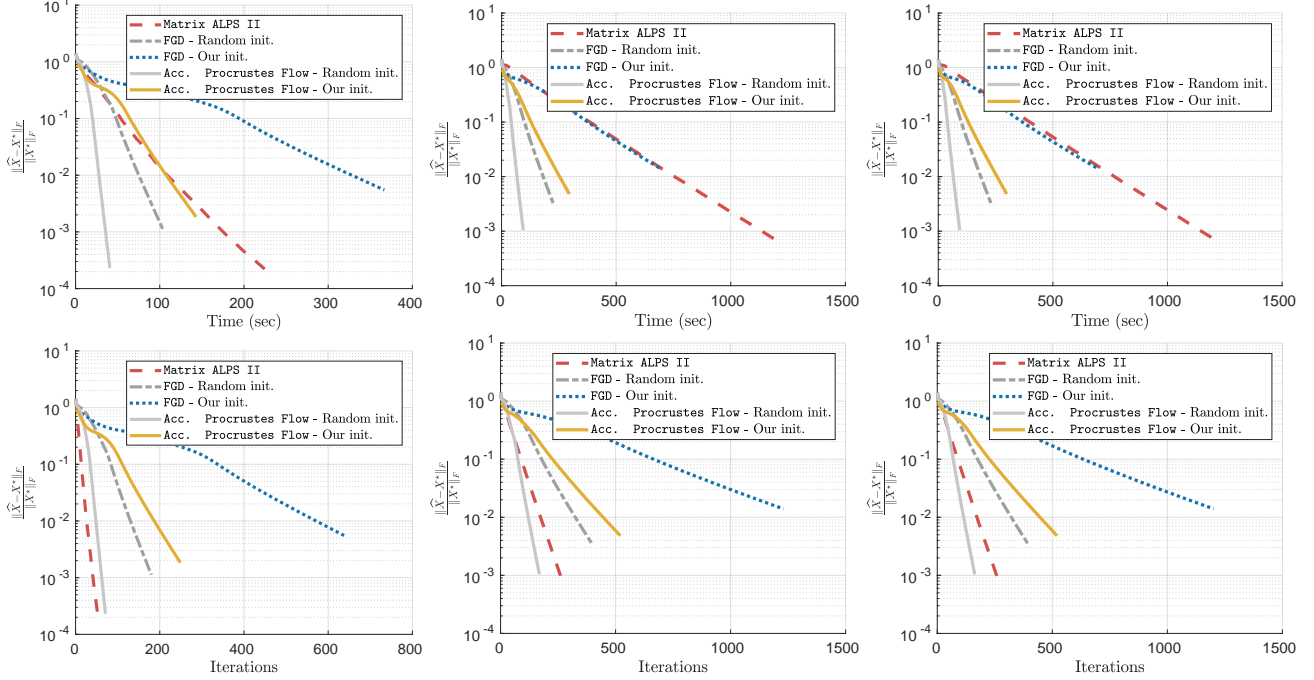


Figure 5: Synthetic example results on low-rank matrix sensing. *Top row*: Convergence behavior vs. time elapsed. *Bottom row*: Convergence behavior vs. number of iterations. *Left panel*: $C = 5$, noiseless case; *Center panel*: $C = 3$, noiseless case; *Right panel*: $C = 3$, noisy case with $\|w\|_2 = 10^{-2}$.

For the simulation, we considered a spiking neural network model with 1000 neurons (200 inhibitory and 800 excitatory neurons). We then simulated 20 seconds of spiking activities for these neurons and sampled these activities at a sampling rate of 200Hz. The input stimulus occurred every 2 seconds and lasted 0.3secs. Hence, the (unknown) neuronal activity matrix X was of size 1000×4200 . The neurons are assumed to be uniformly distributed along the depth between $1\text{-}210\mu\text{m}$ from the surface.

The surface potentials y (single μECoG electrode recording) was then computed from these neuronal potentials using the distance dependent lowpass filtering, where the cutoff frequency $[f_c(d)]$ is defined as in sec. 6, the amplitude attenuated according to the distance, and then summing up the potentials. We chose the distance parameters to be $\Delta_1 = 1, \Delta_2 = 0.25, h = 10$. Note that, these operations (low pass filtering and attenuation) can be combined into a linear transformation $\mathcal{A}(X) = \mathbf{A}\text{vec}(X)$ on the neuronal activity matrix X . The matrix $\mathbf{A} \in \mathbb{R}^{m \times nm}$ is a banded matrix assuming an FIR filter for lowpass filtering. In our case, $m \cdot n = 4.2 \times 10^6$. The objective of the low rank matrix sensing model is to recover the simulated neuronal activity matrix X from the surface potentials y .

The neuronal activity matrix X is low rank with $\text{rank}(X) \leq r$, and can be written as $X = UV^\top$, for $U \in \mathbb{R}^{n \times r}, V \in \mathbb{R}^{m \times r}$. The factorized low rank matrix sensing problem becomes

$$\min_{U \in \mathbb{R}^{n \times r}, V \in \mathbb{R}^{m \times r}} \frac{1}{2} \|\mathcal{A}(UV^\top) - y\|_2^2. \quad (9)$$

Rectangular version of the Procrustes flow algorithm has been studied in [34, 49, 51] to solve the above problem. Here, we consider the following accelerated Procrustes flow:

$$\begin{aligned} U_{i+1} &= Z_i - \eta \mathcal{A}^\dagger(\mathcal{A}(Z_i W_i^\top) - y) \cdot W_i, \\ V_{i+1} &= W_i - \eta \mathcal{A}^\dagger(\mathcal{A}(Z_i W_i^\top) - y)^\top \cdot Z_i, \\ Z_{i+1} &= U_{i+1} + \mu(U_{i+1} - U_i), \\ W_{i+1} &= V_{i+1} + \mu(V_{i+1} - V_i). \end{aligned}$$

Z_i, W_i are the auxiliary variables that accumulate the ‘‘momentum’’ of the variables U, V ; the dimensions are apparent from the context. μ is the momentum parameter that weighs how the previous estimates U_i, V_i will be mixed with the current estimate U_{i+1}, V_{i+1} to generate Z_{i+1}, W_{i+1} . The parameters η and μ and the initial points are selected as in Algorithm 1. The rank $r = 10$ for our data.

Figure 6 plots the recovered potentials (along with the actual membrane potentials) for the four neurons (4 rows of $\hat{X} = \hat{U}\hat{V}^\top$ and X), corresponding to the four neurons discussed in sec. 6 over 20 secs of the simulation. The convergence behavior

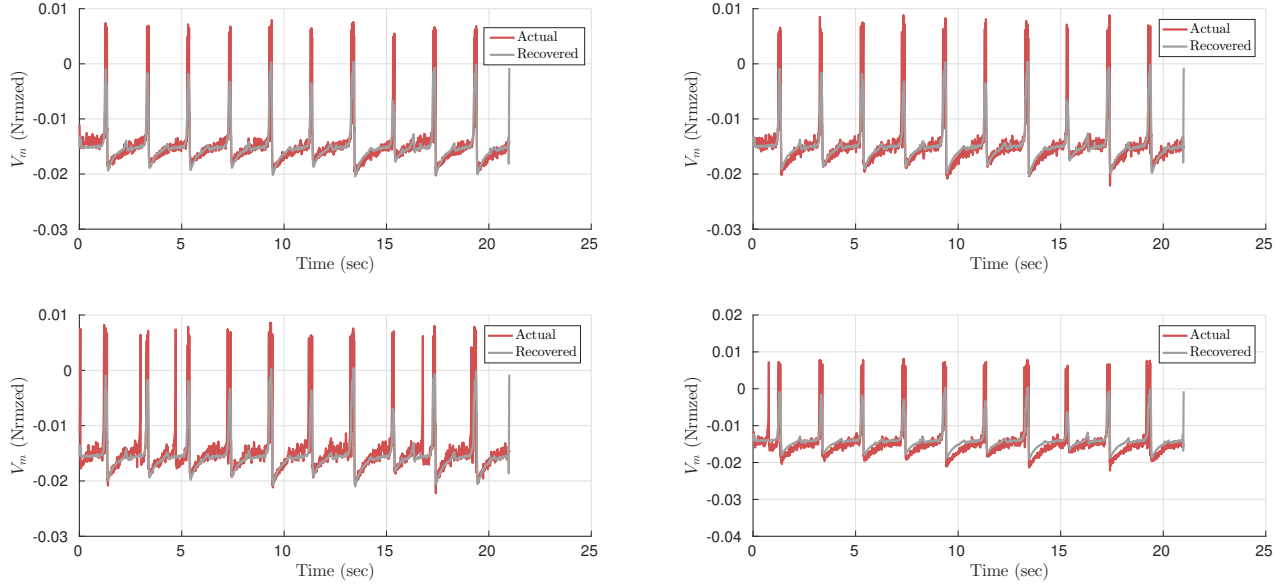


Figure 6: The actual membrane potentials during the 20secs simulation and the recovered potentials for the four neurons.

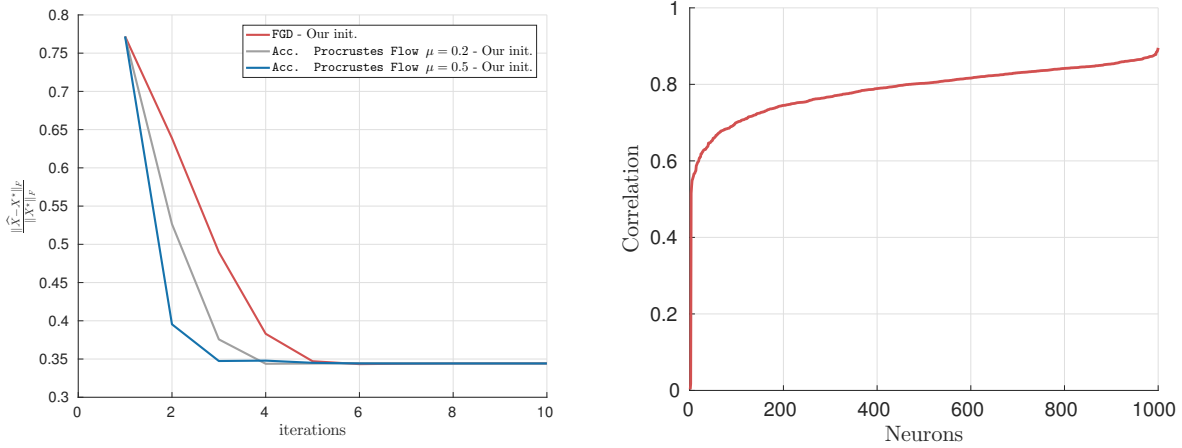


Figure 7: Neuronal activity recovery: Convergence behavior vs. number of iterations (left), Correlation between the recovered and actual membrane potentials for the 1000 neurons (right).

of factored gradient descent (rectangular Procrustes flow) and our accelerated Procrustes flow (with $\mu = 0.2$ and $\mu = 0.5$) algorithms for the neural activity recovery problem are given in the left plot of fig. 7. We also give the correlation between the recovered and actual membrane potentials for the 1000 neurons in the right plot. We note that for most neurons ($\sim 90\%$), the recovered potentials are close to the actual simulated ones.

14 Quantum state tomography

In QST, A_i 's are constructed as q -qubit Pauli observables: *i.e.*, $A_i = \otimes_{j=1}^q s_j$ where \otimes denotes the Kronecker product. Each s_j is a 2×2 matrix from the set:

$$\sigma_I = \begin{bmatrix} 1 & 0 \\ 0 & 1 \end{bmatrix}, \quad \sigma_x = \begin{bmatrix} 0 & 1 \\ 1 & 0 \end{bmatrix}, \quad \sigma_y = \begin{bmatrix} 0 & -i \\ i & 0 \end{bmatrix}, \quad \sigma_z = \begin{bmatrix} 1 & 0 \\ 0 & -1 \end{bmatrix},$$

where i denotes the imaginary number.

There are 4^q such observables in total. In general, one needs to have the expectation values of all 4^q Pauli observables to uniquely reconstruct X^* . However, since we look for pure states X^* in quantum tomography (*i.e.*, low-rank quantum states), we can apply the compressed sensing result [70, 71], that guarantees RIP for \mathcal{A} with high probability:

Lemma 13 (RIP for Pauli measurements [71]). *Let $\mathcal{A} : \mathbb{C}^{2^q \times 2^q} \rightarrow \mathbb{R}^m$ be a linear map, such that $(\mathcal{A}(X^*))_i = \frac{2^q}{\sqrt{m}} \text{Tr}(A_i \cdot X^*)$, where A_i are Pauli operators. Then, with high probability over the choice of $m = \frac{c}{\delta_r^2} \cdot (r2^q q^6)$ Pauli observables A_i , where $c > 0$ is an absolute constant, \mathcal{A} satisfies the r -RIP with constant δ_r , $0 \leq \delta_r < 1$.*

14.1 Setup

We report on the reconstruction of the state of quantum circuits consisting of $q = 6$ qubits, synthesized by the application of CNOT gates on pairs of qubits (GHZ circuit), of Hadamard gates on all qubits (Hadamard circuit) and a random selection of CNOT and U3 gates respectively on pairs of and individual qubits organized in a structure that is 40 levels deep (Random circuit). We use IBM Quantum Information Software Kit (QISKit)⁹ for preparing the circuits and presenting them to QASM Simulator, which is a high performance quantum circuit simulator written in C++ that includes a variety of realistic circuit level noise models (and is included in QISKit)¹⁰.

For each circuit, 8192 pulses were simulated for each of the $4^6 = 4096$ possible measurement circuits (one per Pauli observable) and corresponding measurement tuples (each expressing the distribution of the pulses across $2^6 = 64$ possible binary sequences) were recorded, converted to single-number correlation measurements and subsequently stored. Note that the format of the measurements is identical to those produced by the real quantum device backends accessible online as part of the IBM Q Experience initiative (currently at 5, 16 and 20 qubits)¹¹.

We randomly chose informationally incomplete subsets of the measurements (here 60% of all measurements) and run Algorithm 1 assuming that the reconstructed state \hat{X} is of rank $r = 1$ (pure state); we utilize high-performance Pauli projector operators in the iteration. We test the behavior of our algorithm for different values of Nesterov parameter: $\mu = 0$ (no acceleration) as compared to $\mu = \frac{1}{8}, \frac{1}{4}, \frac{1}{3}, \frac{3}{4}$ and we run each QST experiment for 10 times by randomly varying initial \hat{X} . We record the evolution of error at each step (absolute and relative; with respect to target X^* and between successive iterates) and the fidelity of the reconstruction (defined as the inner product of target and converged states - when these are pure ones - with a value of 1 denoting perfect reconstruction of target state from measurements) and stop when the relative error of successive iterates gets smaller than $\text{reltol} = 5 \times 10^{-4}$ or the number of iterations exceeds 1000 - whichever happens first.

⁹<https://qiskit.org/>

¹⁰<https://www.ibm.com/blogs/research/2018/05/quantum-circuits/>

¹¹<https://quantumexperience.ng.bluemix.net/qx/devices>